# Journal of Materials Chemistry C

Accepted Manuscript


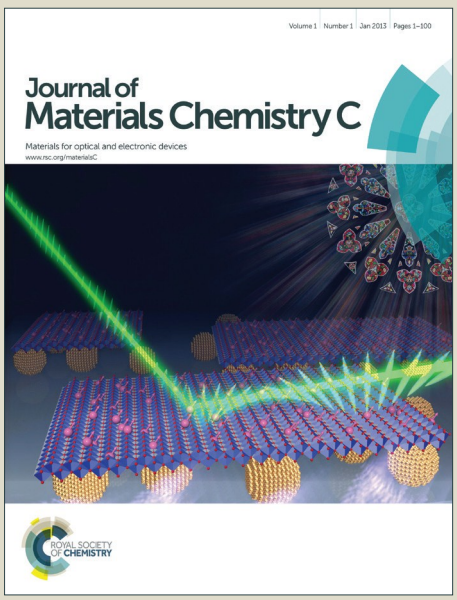





ROYAL SOCIETY OF CHEMISTRY

www.rsc.org/materialsC

# Photonic Crystals for Sensitized Solar Cells: Fabrication, Properties, and Applications

Keyu Xie,*[a] Min Guo,[b] and Haitao Huang*[b]

[a]State Key Laboratory of Solidification Processing and Center for Nano Energy Materials, Northwestern Polytechnical University, Xi'an 710072, P.R. China; E-mail: nwpuxky@163.com

[b]Department of Applied Physics and Materials Research Center, The Hong Kong Polytechnic University, Hung Hom, Kowloon, Hong Kong; E-mail: aphhuang@polyu.edu.hk

**Abstract:** The surging of photovoltaics has witnessed the boost of numerous fascinating approaches to the enhancement of power conversion efficiencies (PCE) of the devices. Coupling photonic crystals (PCs) to photovoltaics is regarded to be effective in photon management and thus PCE enhancement. This review summarizes the recent progress in the fabrication strategies, optical properties, and application fundamentals of PCs for sensitized solar cells, with an emphasis on the relatively new and promising developments. It focuses on the fabrication methods of several major types of PCs that are applicable to sensitized solar cells and their optical properties, as well as the fundamental insights on the role played by the PCs in these solar cells. Also, the advancements in the applications of different types of PCs in various sensitized solar cells, such as liquid-state dye-sensitized solar cells, solid-state dye-sensitized solar cells, quantum-dot sensitized solar cells, and perovskite solar cells, are reviewed. Finally, the future perspectives of PC-based sensitized solar cells are discussed.

Keywords: Photonic Crystal; Photon Management; Sensitized Solar Cells.

## 1. Introduction

One of the greatest challenges in the 21st century is undoubtedly the energy scarcity. It was predicted by the U.S. Energy Information Administration (EIA) that the total world energy consumption would rapidly grow from 505 quadrillion Btu in 2008 to 619 quadrillion Btu in 2020 and 770 quadrillion Btu in 2035.[1] More seriously, the worldwide demand for energy is predicted to double by 2050 and triple by 2100.[2, 3] Fortunately, harvesting nature's energy to meet the worldwide energy demand provides us a great option to overcome this dilemma. Renewable energies, such as hydroelectric, wind, biomass, geothermal, marine tidal and solar energy, are generally acknowledged as alternative energy sources for sustainable development of human society. Increasing the share of renewable energies in the world energy matrix will help prolong the existence of fossil fuel reserves, address the threats posed by climate change, and enable better security of energy supply on a global scale.[4]

Among the above-mentioned renewable energy sources, the solar energy has the potential to provide our planet with about 10,000 times more energy than our global daily consumption.[5] Due to the abundance of solar energy, photovoltaic technology that converts sunlight to electricity, has attracted lots of research interest.[6, 7] Aiming at boosting the efficiency of photovoltaic energy conversion, great efforts have been made to develop advanced solar energy materials and photovoltaic manufacturing technologies.[8, 9]

The concept of photon management has recently emerged as a hot research topic in an effort to enhance light harvesting efficiency in photovoltaics. Nanostructured materials, such as photonic crystals (PCs), large particle aggregation scattering layers, and plasmonic nanometals have opened unprecedented opportunities for light management, notably in the third generation thin-film solar cells.[10-14] PCs, with periodic dielectric nanostructures, show great ability to achieve a new level of control of light propagation and light energy distribution in photovoltaic devices.[15] By coupling PCs into photovoltaic devices, photons will have a greater probability to be absorbed, resulting in increased light harvesting

efficiency in these devices via various mechanisms, such as 1) photon localization and enhanced red light absorption near the red edge of a photonic bandgap,[16] 2) light reflection within the photonic bandgap at various angles,[17] and 3) formation of photon resonance modes within the solar cell.[18] Generally, an improved light harvesting efficiency is likely to result in a higher power conversion efficiency (PCE) of the cell and/or lower usage of absorbing material.[19] Therefore, high-efficiency photovoltaic devices with low-cost are expected.

Currently, sensitized solar cells, such as dye-sensitized solar cells (DSSCs) and quantum-dot sensitized solar cells (QDSCs), are promising low-cost alternatives to traditional photovoltaic devices based on materials such as Si and CdTe,[20, 21] due to their lower material cost, simpler fabrication process, and even lower investment cost. The first demonstration of light absorption enhancement effect of PC integrated sensitized solar cells in 2003 has encouraged more and more attempts to design PCs with different structural and optical properties that allow for light management in the cells.[16] Meanwhile, with the continuous development of nanotechnology, the ability to tailor the optical properties of PCs, and hence the performances of photovoltaic devices, has improved a lot within the last decade. Isolated reports on the experimental and/or theoretical researches have sprung up in recent years, which call for a comprehensive overview of synthesis strategies, optical properties, and application fundamentals of PCs for sensitized solar cells.

The aim of this review is to provide a comprehensive view with a focus on the new and promising developments in the above mentioned areas. Firstly, we will briefly introduce several major types of PCs that are applicable to sensitized solar cells and their fabrication methods. Secondly, we will lay emphasis on the understanding of the optical properties of these PCs and the role played by the PCs in sensitized solar cells. Thirdly, we will summarize the advances in the applications of PCs in sensitized solar cells. Finally, we will point out future research directions for further exploration of PC coupled sensitized solar cells.

## 2. Photonic crystals for sensitized solar cells and their fabrication strategies

PCs can be obtained through periodic arrangements of different dielectric materials and are periodically modulated at sub-wavelength scale in one, two or three dimensions to form a forbidden gap in the photonic band structure within a specific range of frequencies.[22, 23] The photonic bandgap of a PC is mainly governed by the micro/nano spatial structure of the constitute dielectric materials and their refractive index contrast, which endows PC with the ability to manipulate and control the propagation of light.

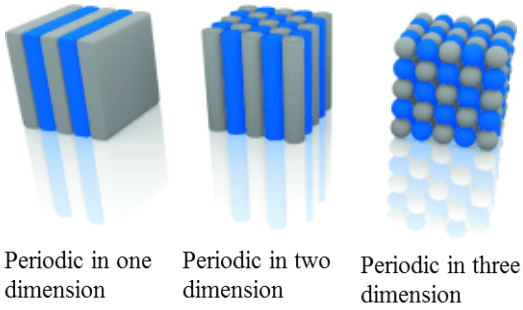


Fig.1 Schematic illustration of three kinds of photonic crystals. Reprinted with permission from ref. 24. Copyright (2014) John Wiley and Sons.

According to the periodic dimensionality, PCs can be broadly classified into three categories: one dimensional (1D), two dimensional (2D) and three dimensional (3D) PCs (Fig. 1). Among them, 1D PCs, also known as Bragg stacks or Bragg reflectors, are consisted of alternating layers of two different materials,[23, 24] where the refractive index is periodically varied in only one dimension but homogeneous in the other two dimensions.[23] For 2D PCs (with columns arranged in a plane crystal lattice structure), the refractive index is varied in two spatial dimensions and constant in the third. For 3D PCs, the most complicated in structures among all three types of PCs, the refractive index is varied in all the three dimensions.[23, 25]

Since the publication of the pioneer theoretical work by Yablonovitch and John in the late

1980s,[26, 27] there has been much interest in exploring new strategies to fabricate artificial PCs and applying them to solar cells, sensors, lasers, light emitting diodes, optical fibers and displays. Some of the typical fabrication techniques, such as evaporation, sputtering, dip/spin-coating, anodic etching, lithography, atomic layer deposition(ALD), chemical vapor deposition (CVD), and so on, can be found in several excellent reviews.[23, 25, 28-31] Herein, we only focus on those PCs that are applicable to sensitized solar cells: (1) 1D multilayer PCs, (2) 3D inverse opal (IO) PCs, and (3) $TiO_2$ nanotube (NT) PCs. The recent development of techniques to integrate these PCs into sensitized solar cells will also be highlighted.

### 2.1 1D multilayer photonic crystals

Layer-by-layer deposition of alternating materials is one of the simplest strategies to fabricate 1D multilayer PCs. The first successful application of 1D multilayer PCs to DSSCs was demonstrated by Míguez and coworkers via coupling a 1D $SiO_2/TiO_2$ multilayer PC to a conventional mesoporous $TiO_2$ layer as the photoanode.[32] The schematic illustration of the fabrication of such a 1D $SiO_2/TiO_2$ PC coupled photoanode is shown in Fig. 2a. The typical fabrication procedure includes the following steps: (1) a mesoporous $TiO_2$ transparent electrode is made by the conventional doctor-blade method; (2) a very thin $TiO_2$ overlayer is first spin-coated on the mesoporous $TiO_2$ film; (3,4) alternate layers of $SiO_2$ and $TiO_2$ colloidal particles are then spin-coated onto the mesoporous $TiO_2$ layer; and (5) the 1D $SiO_2/TiO_2$ PC coupled photoanode is calcined. It is worth noting that, in this fabrication process, two key points should be carefully addressed. The first is the formation of a smooth and uniform $TiO_2$ thin film on the top surface of mesoporous $TiO_2$ layer as mentioned in step (2). In order to achieve resonant modes in DSSCs, which usually play an important role in increasing light harvesting efficiency, an intimate physical contact between the 1D $SiO_2/TiO_2$ PC and the mesoporous $TiO_2$ layer is stringently required.[33, 34] A flat $TiO_2$ overlayer is the prerequisite of the formation of a high-quality 1D $SiO_2/TiO_2$ PC on the mesoporous $TiO_2$

layer. The second is the precise control of the microstructure of 1D $SiO_2/TiO_2$ PC by modulating the concentration of each colloidal suspension and the processing parameters of spin-coating.

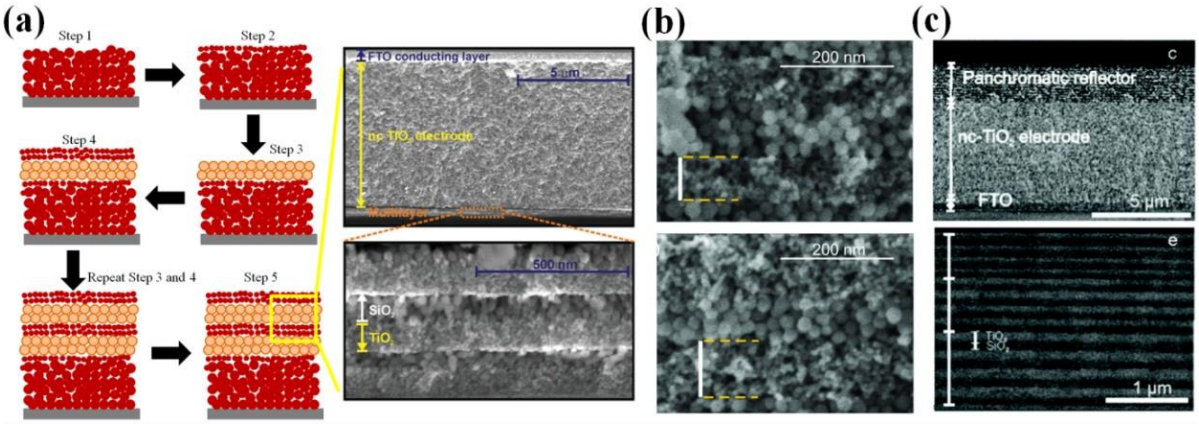


Fig. 2 (a) Schematic of the fabrication process and the SEM images of 1D $SiO_2/TiO_2$ PC coupled photoanode. Reprinted with permission from ref. 32. Copyright (2009) John Wiley and Sons. (b) SEM images of 1D $SiO_2/TiO_2$ PCs with different pore sizes: normal one (top) and larger one (bottom). Reprinted with permission from ref. 35. Copyright (2012) John Wiley and Sons. (c) Structure of 1D $SiO_2/TiO_2$ PC with multi-periodicity. Reprinted with permission from ref. 36. Copyright (2014) Royal Society of Chemistry.

Using the same technique, Míguez *et al*. fabricated a 1D $SiO_2/TiO_2$ PC with enlarged average pore size for better electrolyte diffusion.[35] Polymeric porogenes were incorporated into the $TiO_2$ colloidal suspension to create larger pores after annealing.(Fig.2b). This structural modification of the photoanode further boosts the PCE of the DSSC. Later, a multi-periodicity 1D $SiO_2/TiO_2$ PC has also been integrated to the mesoporous $TiO_2$ layer to form a photoanode.[36] As shown in Fig. 2c, the novel hierarchical PC is constructed by three 1D $SiO_2/TiO_2$ PCs of different periodicities, each with four $SiO_2/TiO_2$ bilayers. The thickness of the bilayer was modulated by the concentrations of $SiO_2$ and $TiO_2$ in the precursor suspensions. This multi-periodicity 1D PC shows a panchromatic reflection in the whole visible range for highly efficient light harvesting in DSSC. In addition, the layer-by-layer

spin-coating method has also been successfully introduced to couple the 1D $SiO_2/TiO_2$ PC to photoanode and counter electrode, respectively, for solid-state DSSCs.[37, 38] Due to its simplicity, this spin-coating method shows great potential in fabricating 1D multilayer PCs for sensitized solar cell applications.

Another strategy to fabricate a novel and conducting 1D $SiO_2$/ITO PC as the counter electrode for sensitized solar cells is reported by Heiniger *et al.*[39] In their work, the $SiO_2$ and ITO multilayer is fabricated by alternating spin-coating and RF magnetron sputtering. Firstly, a $SiO_2$ nanoparticle (NP) layer is spin-coated on the FTO-glass substrate. Secondly, after annealing, an ITO layer is then deposited on the $SiO_2$ layer by RF magnetron sputtering. The above two steps are repeated for several times and the as-prepared 1D $SiO_2$/ITO PC is further annealed in air for counter electrode application. Apart from the high conductivity of the 1D $SiO_2$/ITO PC due to the infiltration of ITO into $SiO_2$, the PC also shows strong reflectance within a certain visible range while preserving semi-transparency in other range.

In addition to the fabrication strategies, more attentions should be paid to the development of 1D PC with new materials, which are suitable for sensitized solar cell applications. In most of above-mentioned cases, the insulating $SiO_2$ will no doubt prohibit the charge transport and make the PC merely a porous reflector. Hence, how to design a new 1D PC with proper alternating materials represents another fruitful research topic for future work in this area.

### 2.2 3D inverse opal photonic crystals

3D IO PCs are the most widely used PCs in sensitized solar cells. As early as 2003, Nishimura *et al.* demonstrated the first 3D IO PC coupled sensitized solar cell.[16] Later, many efforts have been made to identify suitable fabrication strategies to obtain 3D IO PCs with high optical quality for integration into either photoanode or counter electrode of sensitized solar cells. The most well-developed fabrication strategy for 3D IO PCs is the inversion of a self-assembled colloidal crystal template using the target material. A typical

synthesis scheme including relatively straightforward steps is shown in Fig. 3: (1) the self-assembly of colloidal crystals; (2) the infiltration of fluid into the gaps between the templating spheres; (3) the conversion of the fluid into a solid skeleton; (4) the removing of the original template.

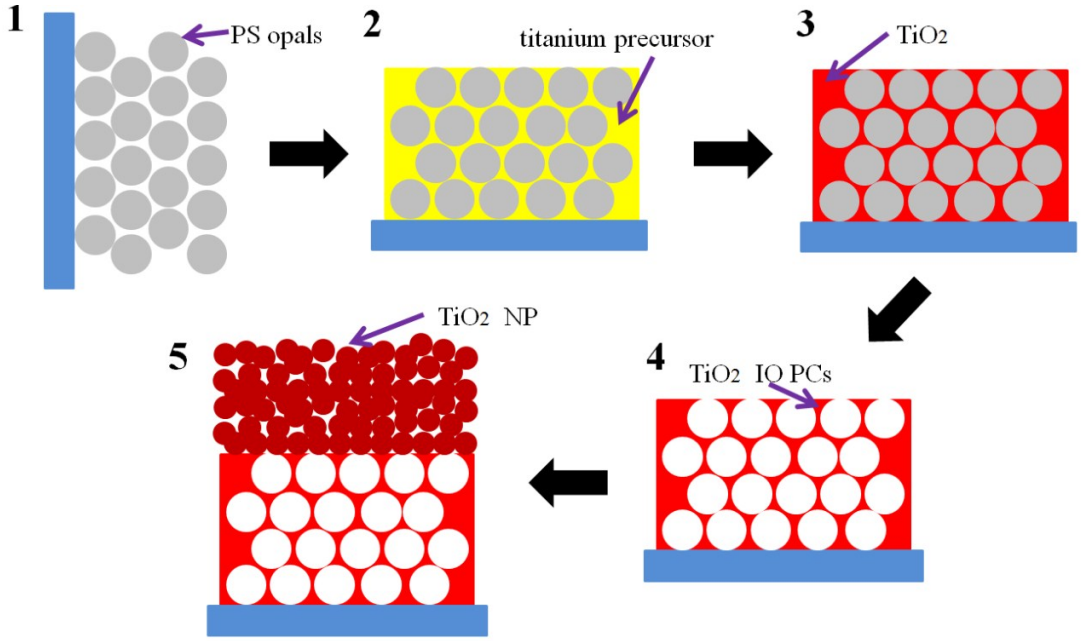


Fig. 3 Schematic illustration of a typical fabrication process of a 3D $TiO_2$ IO PC coupled photoanode.

In the above-mentioned bilayer configuration, enhanced light harvesting is only observed under back side illumination, where the intensity of incident light is greatly reduced due to the strong absorption by the electrolyte. Mihi *et al.* modified the photoanode to allow front side illumination by simply depositing the $TiO_2$ NP absorbing layer on the FTO glass first, followed by the deposition of the 3D $TiO_2$ IO PC layer.

Modifications of the fabrication technologies have been exploited to achieve high quality IO PCs via modifying the key processes of self-assembly and infiltration, where the vertical deposition method is the most widely employed technology in this research realm.[13, 16, 40-49] However, it is time consuming and requires several hours or even a few days to achieve high quality colloidal crystals on a small scale substrate. To scale up, spin/dip-coating or

doctor blade method is introduced.[50-54] Different infiltration methods, such as liquid-phase deposition (LPD),[48, 54, 55] dip/spinning-coating,[41, 45] ALD,[13, 40, 42] and CVD,[42, 43, 53] have been employed to infiltrate precursor or target materials into the pores of the opaline structures. The past decade has seen many self-assembly and infiltration technologies combined to fabricate 3D IO PCs for sensitized solar cells (Tab. 1), which provide us with more design freedoms to best suit a particular application.

Table 1 Typical fabrication technologies of 3D IO PC based sensitized solar cell

| Photoanode | 3D IO PCs Layer | | Absorbing Layer | Ref |
|---|---|---|---|---|
| | Assembly Method + Infiltration Method | | | |
| Single Layer | | | | |
| | Vertical Deposition | + LPD | - | [44, 47, 49] |
| | Vertical Deposition | + Spinning/Dip Coating | - | [41] |
| | Vertical Deposition | + ALD/CVD | - | [13, 40, 43] |
| | Spinning/Dip Coating | + LPD | - | [50-52] |
| | Doctor Blade | + LPD | - | [54] |
| Bilayer | | | | |
| | Vertical Deposition | + LPD | + Doctor Blade | [16, 46, 48] |
| | Vertical Deposition | + Spinning/Dip Coating | + Doctor Blade | [45] |
| | Vertical Deposition | + ALD/CVD | + Doctor Blade/Hydrothermal | [42] |
| | Spinning/Dip Coating | + LPD | + Doctor Blade | [53] |

It is worth mentioning that, in an effort to rapidly obtain large colloidal crystals (centimeter-scale) with relatively low defect levels, a physical confinement method is also developed.[55] In this procedure, the colloidal suspension is first injected into a sandwich type cell by a small positive pressure via a tube. High quality colloidal crystal is then self-assembled on an FTO substrate with the help of sonication (Fig. 4). After LPD of titanium precursor and calcination, anatase 3D $TiO_2$ IO PC is formed on an FTO substrate as the photoanode for a DSSC. Nevertheless, the PCE of the 3D $TiO_2$ IO PC coupled DSSC is only 0.6%. The low PCE is

mainly attributed to the partial infiltration of the titanium precursor into the voids of the opal structure and the volume contraction of the $TiO_2$ film after calcination. Recently, by embedding the voids of self-assembled opals with non-aggregated and highly crystallized $TiO_2$ NPs, a great improvement in packing density of the interstitial volumes of the opal structure was achieved to minimize the volume shrinkage of $TiO_2$ IO PC during calcination.[56] The key point here is the introduction of the organic-layer-coated and highly crystallized $TiO_2$ NPs. The organic coating layer benefits the good dispersion of $TiO_2$ NPs in solution, which results in a dense filling in the interstitial volumes among the polystyrene (PS) particles.

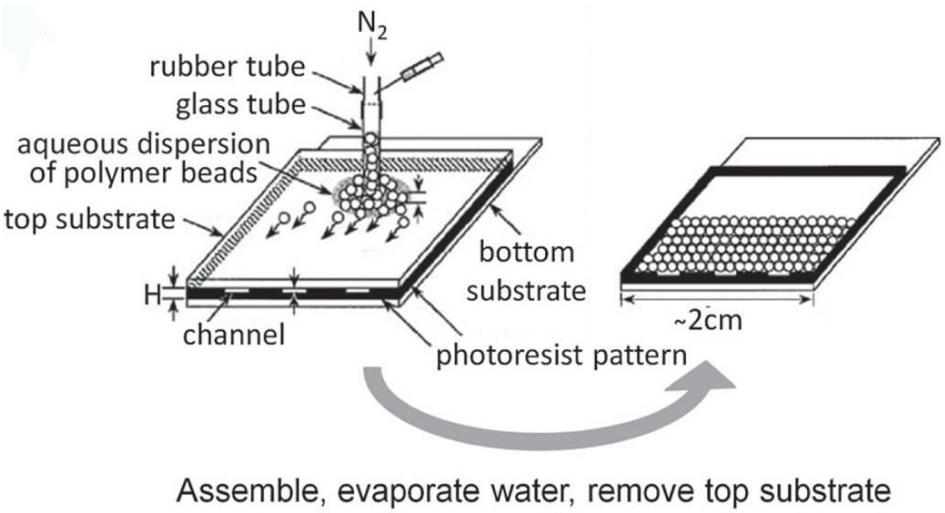


Fig. 4 Schematic illustration of a fabrication procedure of a 3D $TiO_2$ IO PC with physical confinement. Reprinted with permission from ref. 29. Copyright (2013) Royal Society of Chemistry.

As described above, the fabrication procedures for IO PCs involve multistep and are time-consuming. To conquer this challenge, doctor blade deposition method, which is frequently used to fabricate conventional $TiO_2$ nanocrystal film, is used to co-deposit PS template with precursor solution or target materials,[57, 58] and thus, significantly reduce the number of processing steps and time. Combined with the aforementioned physical confinement method,

a co-deposition process involving PS template and $TiO_2$ NPs in a sandwich type cell allows the fabrication of centimeter-scale 3D $TiO_2$ IO PCs within half an hour (Fig. 5a-c ).[59] However, the degree of ordering of the IO structure decreases accordingly. A randomly packed structure of the bottom layer is found to attach the well-ordered structure of the upper layers (Fig. 5d-f), which is common in the rapid co-deposition process.[60] Hence, how to achieve a delicate balance between the fabrication efficiency and the ordering of the IO structure is a challenge.

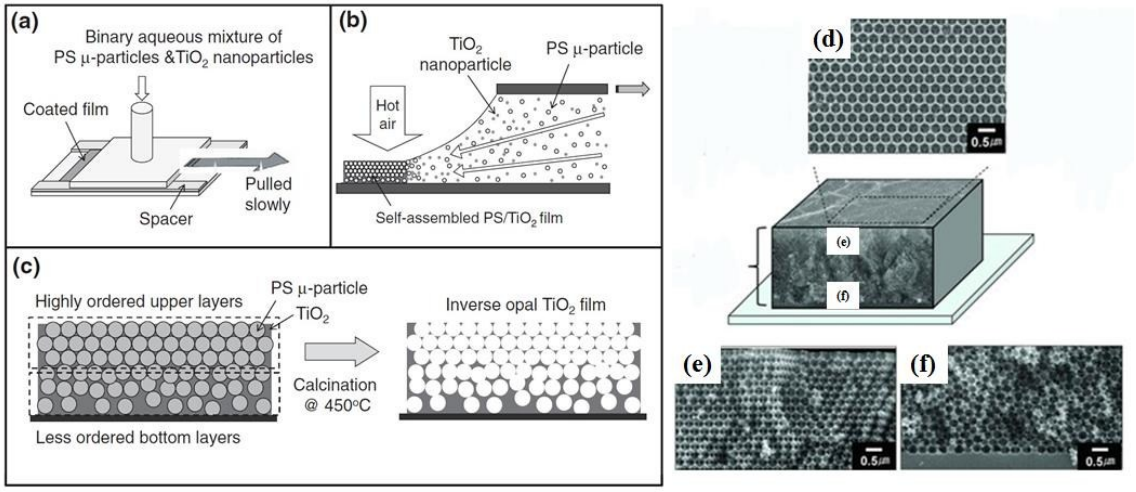


Fig. 5 (a-c) Schematic representation of the co-deposition process of PS templates and $TiO_2$ NPs, combined with the physical confinement method. (d-f) The obtained structures with randomly packed bottom layer and well-ordered upper layer. Reprinted with permission from ref. 59. Copyright (2011) John Wiley and Sons.

### 2.3 $TiO_2$ nanotube photonic crystals

Anodic $TiO_2$ nanotube (NT) array, as one of the one-dimensional nanostructures, has become an attractive photoanode material, due to its potential to considerably accelerate the one-dimensional electron transport along wall of NT which has reduced grain boundaries as compared with the random pathway in a $TiO_2$ NP layer. In addition, it is believed that NTs will be superior to nanorods or nanowires, because of the availability of inner and outer walls of tubes for dye adsorption.[61]

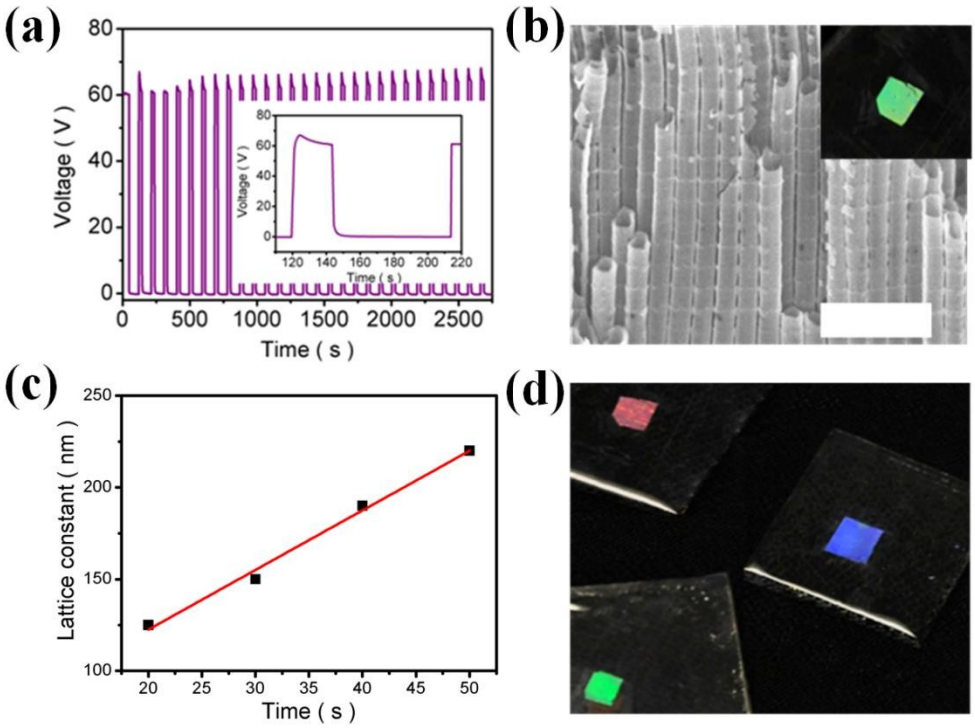


Fig. 6 (a) Typical voltage–time ( *V* - *t* ) transient to fabricate the PC layer. Inset: an enlarged *V* - *t* curve. Reprinted with permission from ref. 63. Copyright (2011) John Wiley and Sons. (b) Cross-section image of the fabricated PC layer. The scale bar measures 1μm. Inset: the PC layer transferred onto a FTO substrate showing a green color. Reprinted with permission from ref. 63. Copyright (2011) John Wiley and Sons. (c) Linear dependence of the lattice constant of the PC on the HC pulse duration. Reprinted with permission from ref. 62. Copyright (2012) Royal Society of Chemistry. (d) Photographs of PC samples (in ethanol) of various colors. Reprinted with permission from ref. 63. Copyright (2011) John Wiley and Sons.

Our group is pioneered in developing a new strategy to couple a $TiO_2$ NT PC to the DSSC photoanode.[62, 63] The novel $TiO_2$ NT PC structure is actually $TiO_2$ NTs with periodicities along the axial direction of NTs fabricated by a periodic current-pulse anodization process (Fig 6a and 6b). Fig 6a displays the current pulse used in the anodization process, where the alternating high current (HC) and low current (LC) was adopted to get $TiO_2$ NTs with different periodicities. The number of pulses and the pulse duration determine the number of periods and the lattice constant, respectively, of the PC layer, and hence the optical properties.

The obtained $TiO_2$ NT PC has great potential for application in sensitized solar cells, because this PC structure and its fabrication method can avoid many drawbacks of the conventional PC structures, such as embedded insulating layer and clogging channels. Apart from the fast electron transport in the NT structure, the $TiO_2$ NT PC is attractive for its freely tunable photonic bandgap which can be easily adjusted by the anodic current pulse duration. The lattice constant of the $TiO_2$ NT PC layer is almost linearly dependent on the HC pulse duration (Fig. 6c) and PC membranes of various color covering the whole visible spectrum can be obtained (Fig. 6d). The freely adjustable bandgap of the $TiO_2$ NT PC allows us to best match the absorption range of any dye molecules or quantum dots for optimized efficiency in sensitized solar cell applications.

Nevertheless, normal PC with a periodic structure only shows a strong reflection of light in a relatively narrow range. To maximize the light harvesting for sensitized solar cells, a strong light reflection over a broader range is preferred. From the structural point of view, this requires a spatial variation of the periodicity where the PC can be called aperiodic PC (APC).[64] Study on APCs with aperiodic sequences, such as, Fibonacci, Cantor, Thue-Morse, and Rudin-Sphapiro, were originally driven by mathematical motivations and previous work was mainly theoretical.[65] Experimentally, due to the lack of an efficient fabrication technique to deal with the extremely complex spatial structure, the existence of large amount of structural defects makes the APCs difficult to accurately display the desired properties.[57, 64, 66, 67]

Recently, the successful fabrication of $TiO_2$ NT APCs (NT APCs) has been demonstrated by using a time-diminishing current-pulse anodization process by our group.[68] During the anodization process, the time duration of the HC pulse is decreased gradually, following an arithmetic sequence (Fig. 7a). As a result, the $TiO_2$ NT APC with a gradually decreasing lattice constant from ~230 nm on the top to ~180 nm in the middle and ~110 nm on the

bottom, respectively, is fabricated (Fig. 7b). Compared with $TiO_2$ NT PC, the $TiO_2$ NT APC shows a broader peak within nearly the full-visible-spectrum from purple to red.

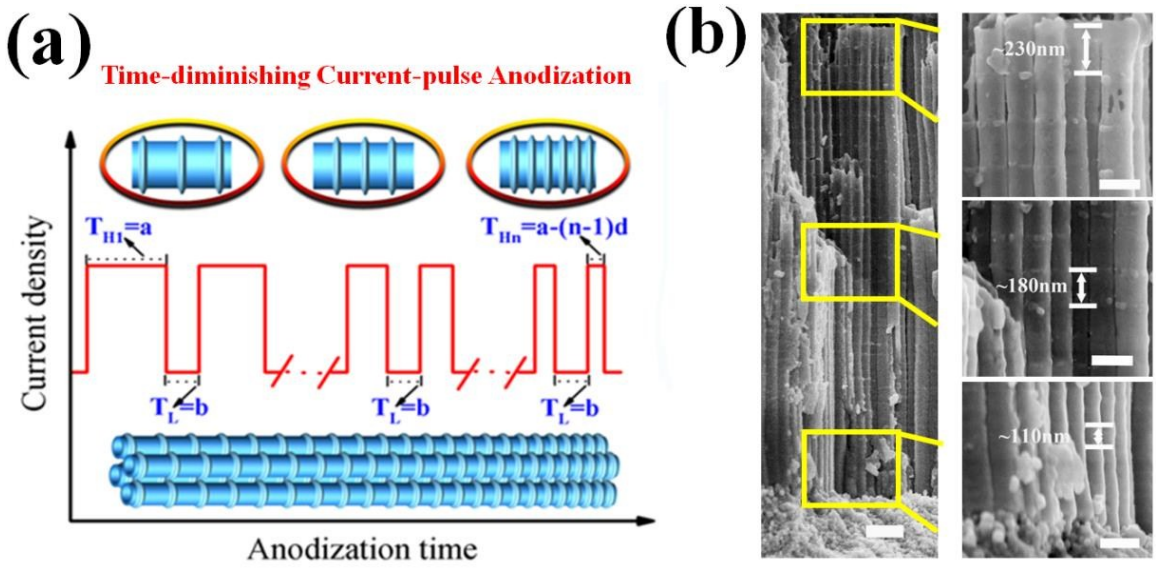


Fig. 7 (a) The time-diminishing current-pulse anodization process for $TiO_2$ NT APC. (b) FESEM image showing the cross-section of a $TiO_2$ NT APC with 35 periods (left, the scale bar measures 500 nm). Magnified views of the $TiO_2$ NTAPC (right, from the top to bottom, the scale bars measure 200 nm). Reprinted with permission from ref. 68. Copyright (2014) Nature Publishing Group.

In short, it is believed that, with the simple, high-controllable and versatile properties, anodization is a powerful tool to fabricate $TiO_2$ NT PC/APCs, and this fabrication strategy offers multi-degree of freedoms in the design of nanostructures for the exploration of a plethora of fascinating properties of PC/APC for practical applications in photonics.

### 2.4 2D photonic crystals

In view of the fairly easy fabrication of 2D PCs with a full photonic bandgap in the visible range by using lithography, various $TiO_2$ 2D PCs (i.e., $TiO_2$ slabs with cylindrical, square and hexagonal columns connected with/without walls and filled with acetonitrile) were proposed by Matsushita *et al*.[69,70] According to their simulation results, the authors experimentally

demonstrated the fabrication of a full-photonic-bandgap structure of a (001) rutile $TiO_2$ substrate by deep reactive ion etching using $SF_6$ plasma.[71] Nevertheless, the 2D $TiO_2$ PC coupled sensitized solar cells as well as the PCE of these solar cells have not been reported yet till now and more effort should be made to explore the applications of 2D PCs.

## 3 Fundamentals of photonic crystals for sensitized solar cells

### 3.1 Optic properties of photonic crystals for sensitized solar cells

The light propagation in PCs can be described by an electromagnetic wave equation, derived from the Maxwell's equations,[28]

$$\nabla \times \left[\frac{1}{\varepsilon(r)}\nabla \times \boldsymbol{H}(\boldsymbol{r})\right] = \left(\frac{\omega}{c}\right)^2 \boldsymbol{H}(\boldsymbol{r}) \quad (3.1)$$

where $\boldsymbol{H}$ and $\varepsilon$ represent the magnetic field and the relative dielectric constant of the media, respectively. The optical response of PCs can be derived by the eigenvalues on the right hand side after the introduction of the spatial dependence of $\varepsilon$ which corresponds to the periodic structure of PCs. As a result, the periodicity of the refractive index in PCs leads to an opening of a gap in the photonic band structure, known as photonic bandgap, just like Bragg-condition for X-ray diffraction, but in optical wavelengths. Photons with frequencies in the bandgap are forbidden, and the unique band structure of PCs will strongly influence the light propagation in PCs. Usually, optical reflection and transmission spectra are employed as tools to characterize the bandgap of PCs, in which light beams are reflected leading to a dip in transmittance and a peak in reflectance.

The optical properties of 1D multilayer PCs depend on the refractive index contrast of alternative layers of different materials/structures and the total number of layers. To attain intense and wide reflection peak, large refractive index contrast is required. $SiO_2$ and $TiO_2$ are typically preferred due to their very different refractive indices and easy fabrication of

uniform thin films. The position of reflection peak (under normal incidence) is determined by the optical thickness of the unit cell,[72]

$$\lambda_{max} = 2nd \tag{3.2}$$

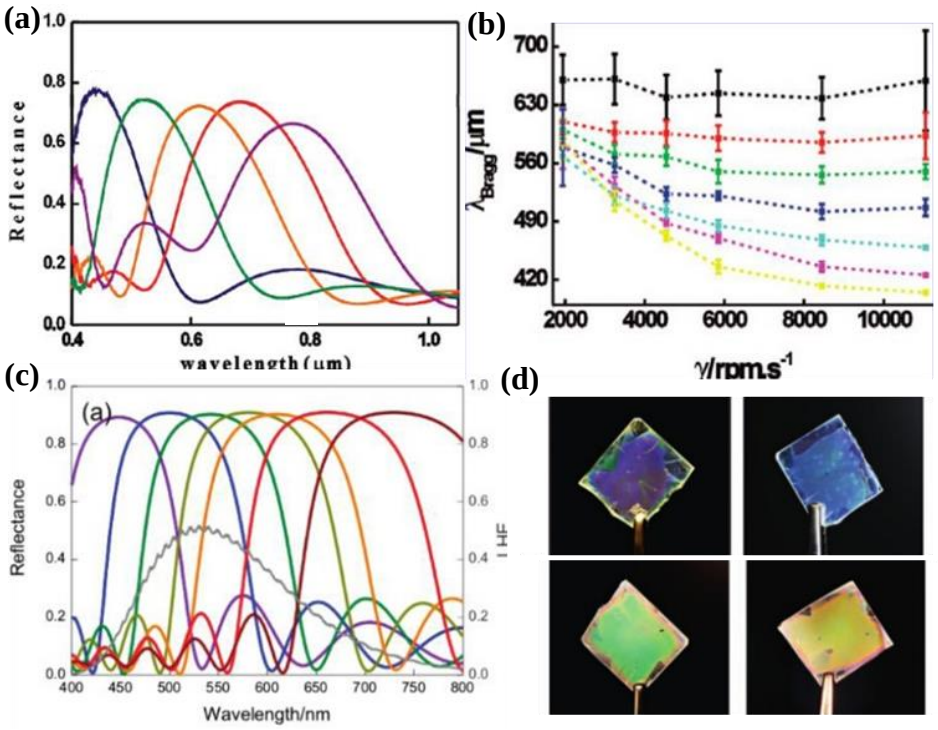


Fig. 8 (a) Experimental reflectance spectra of 1D $SiO_2/TiO_2$ PCs deposited by spin-coating. In all cases, three unit cells of the alternating layers are stacked. Reprinted with permission from ref. 74. Copyright (2008) American Chemical Society. (b) Evolution of the Bragg peak position with the final rotation speed and ramp stage acceleration used in the spin-coating process. Reprinted with permission from ref. 75. Copyright (2009) American Chemical Society. (c) Theoretical specular reflectance for a 14-layer 1D PC with different layer thickness. Reprinted with permission from ref. 76. Copyright (2010) American Chemical Society. (d) Photos of 1D PCs with different colors obtained by varying the layer thickness. Reprinted with permission from ref. 77. Copyright (2011) John Wiley and Sons.

where $\lambda_{max}$ and $d$ are the central wavelength of the reflection peak and the lattice constant of the 1D PC. $n$ is the effective refractive index of the multilayer structure,[73]

$$n = \frac{t_1 n_1 + t_2 n_2}{d} \quad (3.3)$$

where $t_1$ and $t_2$, $n_1$ and $n_2$ present the thicknesses and refractive indices of the two neighbouring layers, respectively.

As a result, the Bragg reflection peak blue shifts as the optical thickness decreases (Fig. 8a-b).[74, 75] Theoretical prediction of the evolution of reflection peak *vs.* the optical thickness is shown in Fig. 8c, in good agreement with the experimental results,[76] and also verified by naked eyes (Fig. 8d).[77] Increasing the total number of unit cells gives rise to more intense and narrower reflection peak, but no shift in position (Fig. 9a).[74] Fig.9b shows the panchromatic reflection spectrum, which is obtained by building 1D $SiO_2/TiO_2$ PCs with multiple periodicities whose fabrication process has been described in above section.[36]

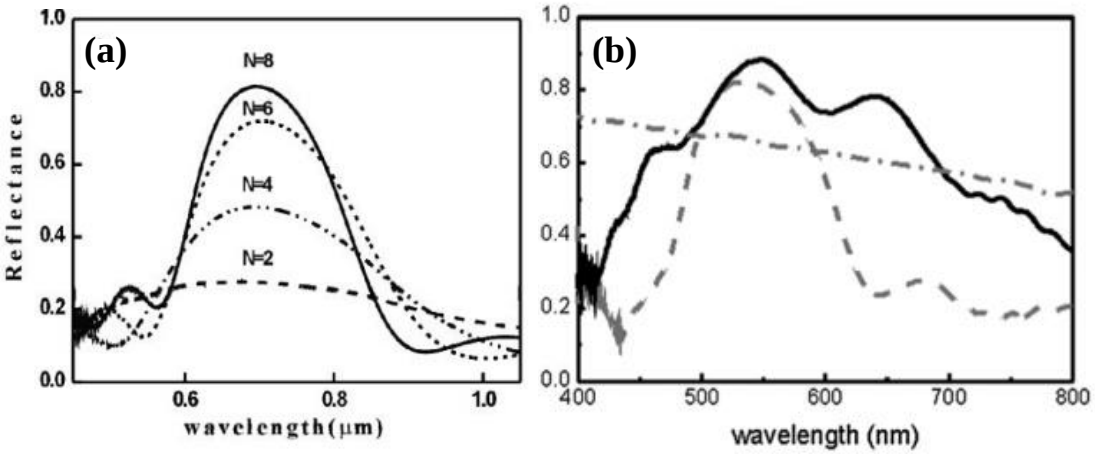


Fig. 9 (a) Experimental reflectance spectra of 1D $SiO_2/TiO_2$ PCs with the different number of deposited layers (N). Reprinted with permission from ref. 74. Copyright (2008) American Chemical Society. (b) Experimental panchromatic reflection spectrum of 1D PC built on triple-period structure (black line), compared with that of 1D PC with a single period (grey dashed line) and a traditional diffuse scattering layer (grey dashed-dotted line). Reprinted with permission from ref. 36. Copyright (2014) Royal Society of Chemistry.

The Bragg position of the IO film is originated from the refractive index contrast between the background medium (air/electrolyte) and the target material, where the spherical cavities

are ordered in a face-centered cubic (fcc) lattice. Therefore, the IO structure is called a 3D PC with varied refractive index in all three spatial dimensions. The optical properties of this 3D PC structure is highly dependent on the periodic size and shape. The position of the Bragg reflection peak can be estimated using the modified Bragg equation when the incident light is normal to the {111} plane[59]

$$\lambda_{max} = 2d_{111}.n_{eff}$$
$$= \left(\frac{8}{3}\right)^{\frac{1}{2}}\left(\frac{D}{m}\right)(f_1.n_1^2 + f_2.n_2^2)^{\frac{1}{2}}$$
$$= 1.633.\frac{D}{m}.(f_1.n_1^2 + f_2.n_2^2)^{\frac{1}{2}} \quad (3.4)$$

where $d_{111}$ is {111} plane spacing of the fcc structure, $D$ is the diameter of the spherical cavity (or the PS microsphere template used in the fabrication process), and $m$ is the order of the reflections (usually the first order reflection $m$=1 is considered). $n_{eff}$ is the effective refractive index of the IO film, which can be calculated by the refractive indices of the target material and the cavities, $n_1$ and $n_2$ respectively, and their volume filling factors, $f_1$ and $f_2$, respectively. $TiO_2$ is regarded as the most promising material to build 3D IO PCs for sensitized solar cells due to its relatively high refractive index and compatible electronic band structure. Thus, the position of the Bragg reflection peak can only be varied by the diameter of cavity of the IO film, which is mainly determined by the diameter of the PS used. Fig. 10 shows the evolution of the reflectance spectra with the sphere diameter, where a linearly relationship is observed.[78] It should be noted that due to the shrinkage of the film during calcination for the removal of PS, the peak position may move to shorter wavelength than the calculated one according to Eq. 3.4. Increasing the thickness of the IO film leads to an obvious increase in reflectance intensity due to multiple reflections and interferences.[79] Specifically, a slight red shift of the reflection peak is also observed with increasing film thickness, due to the finite-size of PC and the substrate effect.[79] Due to the different wavelengths covered by photonic stop band, various colors of the IO films, spanned from violet to red, are

obtained.[59] Moreover, by integrating two IO films of different Bragg positions in a tandem structure, Míguez *et al.* has also broadened the spectral reflection range of the IO PC (Fig. 11a).[53]

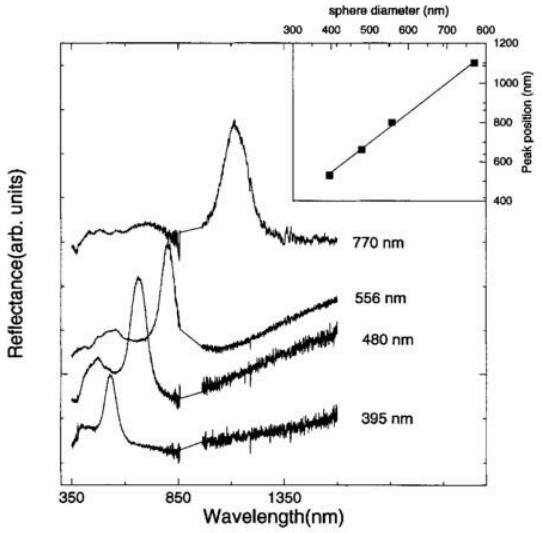


Fig.10 Experimental reflectance spectra of IO PCs made of different diameters of template spheres. The inset shows the linear dependence of the peak position on the sphere diameter. Reprinted with permission from ref. 78. Copyright (2001) John Wiley and Sons.

Compared with the 1D multilayer PCs, the IO PCs normally show a high reflectance at shorter wavelengths due to the inevitable cracks in the films which form the sources of scattering. Other scattering sources for IO films result from the lower level of ordering than desired. The disorders also lead to thinner effective thickness than the actual one since only certain layers of IO structure contribute to the PC effect. For example, due to the disordered pore layers near the substrate, Lee *et al.* observed a much lower reflection peak from the back side (substrate side) than that from the front side (Fig. 11b).[59] As disorders cause unwanted scattering, additional efforts to reduce disorders in IO structure should be made to obtain good spectrally selective reflection.[80]

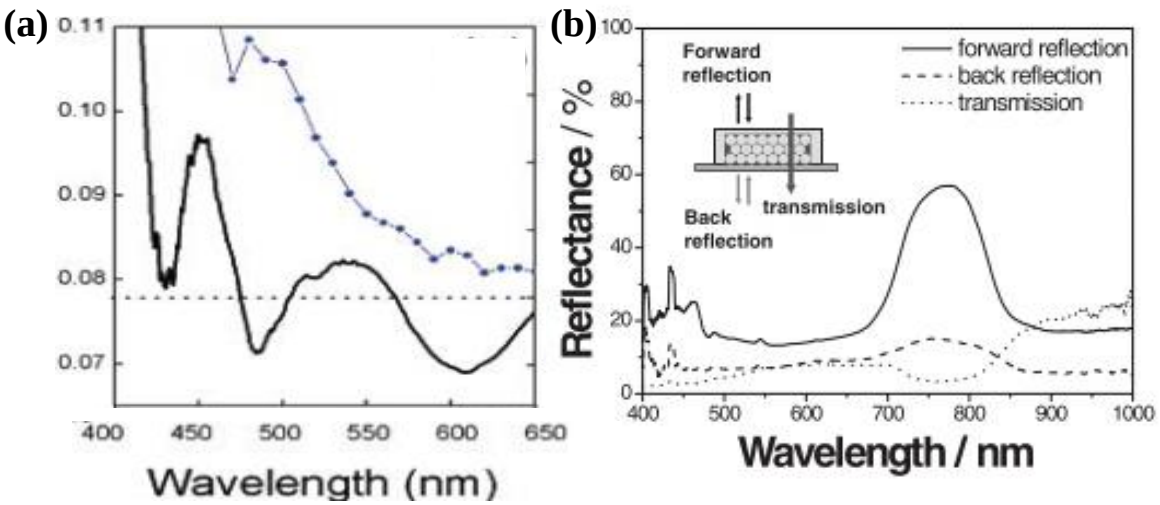


Fig. 11 (a) Specular reflectance spectrum of a photoanode containing two IO structures with different cavity diameters (black line). Reprinted with permission from ref. 53. Copyright (2008) American Chemical Society. (b) The different reflectance spectra obtained from both sides of the IO film. Reprinted with permission from ref. 59. Copyright (2011) John Wiley and Sons.

For $TiO_2$ NT PCs, the Bragg position can be tuned by changing the lattice constant of the PC through adjusting the anodization parameters. Taking the current-pulse anodization as an example, Fig. 6c shows the lattice constant can be controlled by the duration of the high current pulse, resulting in different colors of the $TiO_2$ NT PC films (Fig. 6d).[81] The experimental results agree well with the simulated reflectance spectra of the $TiO_2$ NT PC in terms of peak position. As shown in Fig. 12a, the reflectance spectra sweeps from less than 400 to 730 nm when the axial lattice constant is increased from 110 to 210 nm, showing a good tunability to cover the whole visible range. Besides the peak position, the width of reflection peak slightly increases while the peak intensity slightly decreases with increasing lattice constant, mainly due to the reduced number of unit cells in an NT PC layer when the total thickness of the PC layer is fixed.

In the NT PC structure, the diameter of the $TiO_2$ NTs also plays a key role in determining the photonic band structure of the NT PCs. Fig. 12b displays the calculated reflectance spectra of $TiO_2$ NT PC layers with different diameters of NTs, which can be also easily controlled by the anodization voltage in practice.[82] Interestingly, the position and width of the Bragg peak show noticeable changes with the diameter of the $TiO_2$ NTs, leaving plenty of opportunities in design and optimization of the $TiO_2$ NT PC for sensitized solar cells via fine tuning of the nanostructures. Particularly, when the $TiO_2$ NT diameter decreases from 190 to 70 nm, the Bragg reflection peak red-shifts from 495 to 555 nm, and its width is dramatically broadened by twice, which is believed to be resulted from the increased effective refractive index of the $TiO_2$ NT PC layer. The easily tunable Bragg peak (in terms of position, width and intensity) offers great opportunities for the optimization of sensitized solar cells.

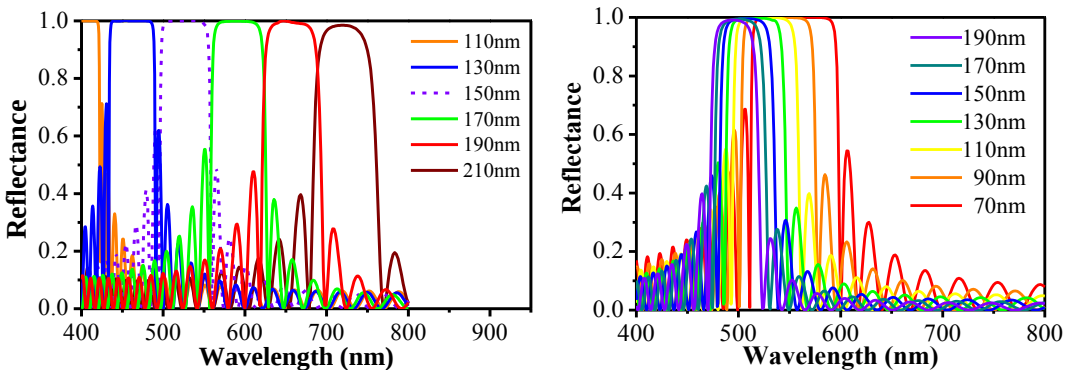


Fig. 12 (a) Calculated reflectance spectra of $TiO_2$ NT PC layers (thickness fixed at 4.5 μm) with different axial lattice constants. (b) Calculated reflectance spectra of $TiO_2$ NT PC layers with different diameters of NTs. The axial lattice constant is fixed at 150 nm. Reprinted with permission from ref. 82. Copyright (2013) American Chemical Society.

### 3.2 Functionalities of PCs in sensitized solar cells

The aim of light trapping strategies for solar cells is to improve the photo-generated current by prolonging the light-material interaction time and hence efficiently utilize the solar spectrum. The increased photo-generated current actually originates from the enhanced light

harvesting efficiency (LHE), which is defined as the fraction of light intensity absorbed by the sensitizer at a certain wavelength,[83, 84]

$$\text{LHE}=A=I_A/I_0 \quad (3.5)$$

where $A$ is absorptance, $I_A$ is the absorbed intensity and $I_0$ is the incident one.

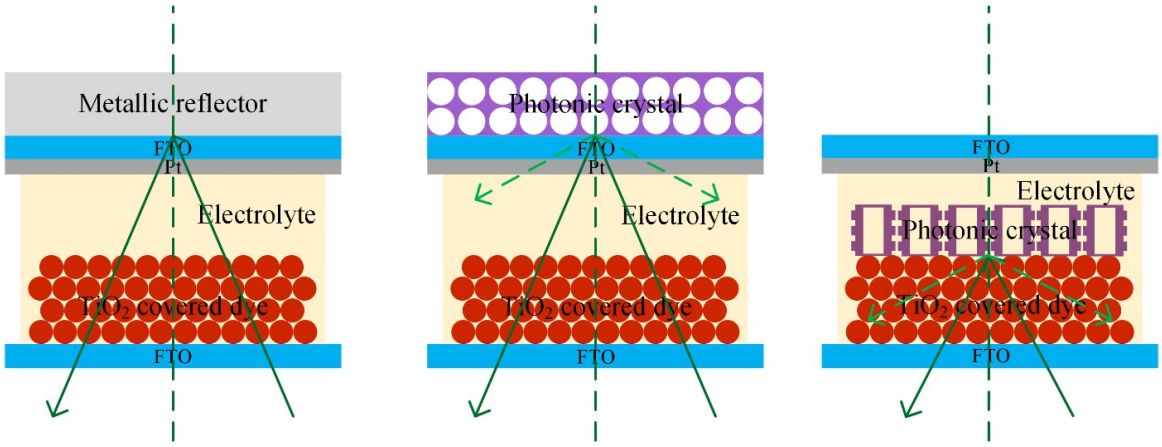


Fig. 13 Schematic illustration of solar cells with (a) a back-side mirror, (b) a back-side PC, and (c) a bilayer-architectured PC coupled photoanode.

Among the various optical designs for sensitized solar cells, a conventional approach is to increase the optical path length by using a simple back-side mirror (Fig. 13a). This geometrical optics method almost equally reflects light of different wavelengths back to the mesoporous $TiO_2$ layer. The employing of PCs, as one of the wave optics approaches, can reflect or diffract unabsorbed photons only in a desired wavelength range (Fig. 13b). A key advantage of wavelength-selective PC reflectors, compared with the traditional metallic reflectors, is their transparency or semi-transparency outside the stop bands of PCs.[85] In addition, PCs can be designed to diffract incoming light into highly oblique angles, which also lengthen the optical path in cells. When the angle of diffracted beam is larger than the critical angle, the beam will also be total internally reflected inside the cells.[17, 86]

PCs for sensitized solar cells are typically made of porous nanostructures, unlike the geometrical optics reflectors which is commonly dense, making them suitable for direct

integration to the photoanode for the permissive electrolyte transport through the PC films (Fig. 13c).[87] By doing so, significant photon intensity loss due to the absorption by the electrolyte and probably the counter-electrode can be reduced, as compared with the use of a metallic back mirror (Fig. 13a). A bilayered architecture of photoanode, consisting of an absorbing layer and a PC reflecting layer, has been demonstrated to be the most beneficial rout for achieving high efficiency DSSCs.[43, 62, 89] Particulalrly for $TiO_2$ NT PC coupled DSSC,[82] the simulated reflectance of the $TiO_2$ NT PC, the absorbtance of the PC coupled DSSC and the wavelength dependent electric field distribution in the integrated photoanode (Fig. 14) show that the enhacnment effect of NT PC is mainly attributed to strong localization of the electric field in the absorbing film caused by back-reflection from PC in stop band and a Fabry-Perot cavity like behavior of PC, resulting in a huge field envelope in NT PC layer at two band edges (Fig. 14c). Miguez *et al.* studied the functional mechanism of 1D $SiO_2/TiO_2$ PC and 3D $TiO_2$ IO PC in bi-layered architectured DSSCs. Similar mechanisms of the absorption amplification in PCs' stop band were found by spectra simulation and electric field distribution analysis.[76, 83] The position of the absorptance peak was found to match the dip in reflectance curve, which was due to the optical resonant modes localized in the absorbing layer.[83, 90]

Near the blue and red edges of a photonic bandgap, the group velocity ($d\omega/dk$) of a photon is significantly reduced (Fig. 15a).[16, 44, 63] These 'heavy' or 'slow' photons will contribute to the LHE enhancement due to the increased matter-photon interaction time. Light localization in the high refractive index part (for photons at the red edge of the bandgap) or the low refractive index part (for photons at the blue edge of the bandgap) was also proposed to be one of the mechanisms for increased LHE in particularly the $TiO_2$ NT PC coupled DSSC, due to its semiconducting nature (Fig. 15b).[41, 63, 79] Moreover, the diffuse light scattering caused by cracks and/or disorders in real PCs and multiple internal reflection/scattering may also give rise to the LHE increasing (Fig. 15c).[44, 62]

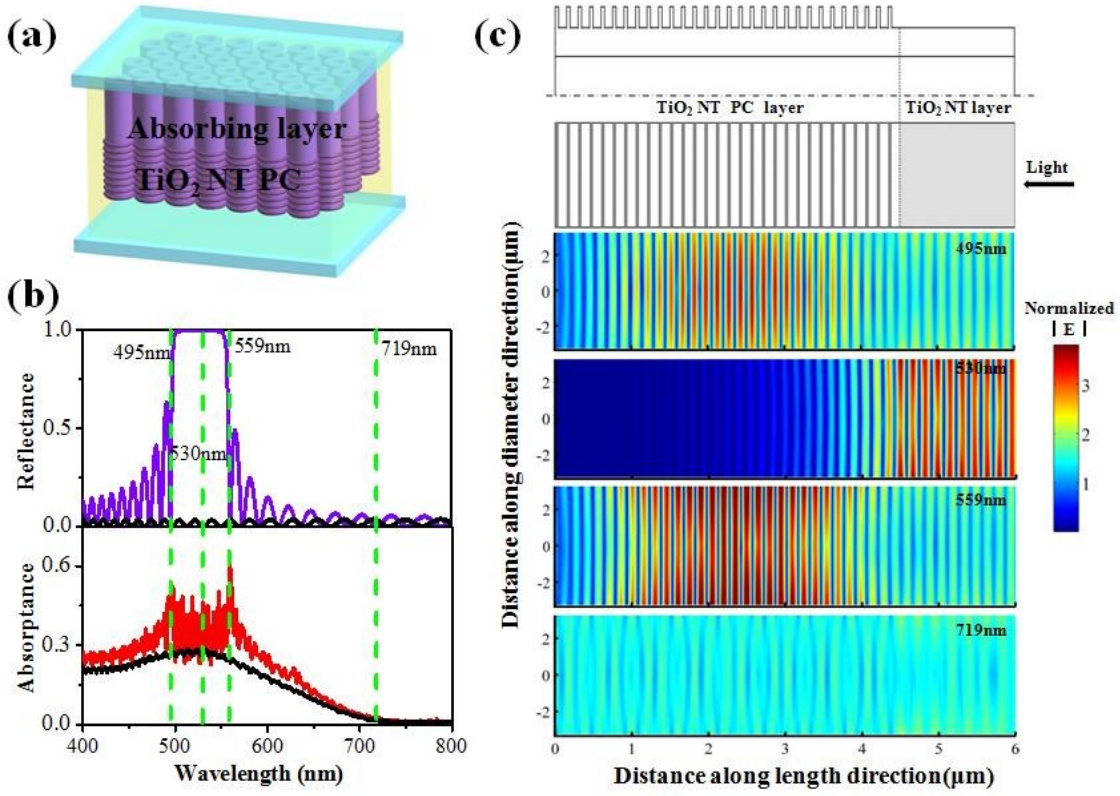


Fig. 14 (a) Design of the DSSC based on a bi-layered photoanode, consisting of an absorbing layer (normally $TiO_2$ NT layer) and a $TiO_2$ NT PC layer. (b) Calculated reflectance, absorptance of the PC layer and integrated DSSC, respectively. (c) The spatial distribution of the squared amplitude of the electric field of the photoanode at four selected wavelengths. Reprinted with permission from ref. 82. Copyright (2013) American Chemical Society.

There are extra benefits brought about by the coupling of PC structures. According to Bragg's law, $\lambda_{peak} = 2d \times n_{eff} \times sin\theta$ (where $d$ is the lattice constant of PC, $n_{eff}$ is the effective refractive index, and $\theta$ is the angle between the incident light and the periodic planes), the Bragg peak position $\lambda_{peak}$ should blue shift as the incident angle increases (incident angle = 90°–$\theta$).[91] This feature can be used for reducing the angular dependence of a sensitized solar cell.[73, 87] As illustrated in our previous work, by coupling the photoanode with $TiO_2$ NT PC, the reduced angular dependence of the power output can be achieved through two strategies: (1) purposely choose the Bragg position to be located at the longer wavelength side

of the dye absorption peak. When the incident light is tilted, the Bragg peak will blue shift, having more overlap with the dye absorption peak, and hence harvest more efficiently the incident light. This partially compensates the reduced photon flux due to light inclination; and (2) when the incident light is tilted, the photons will encounter more interfaces between the walls of NTs and be scattered. The enhanced light scattering also compensates the power loss due to the reduced photon flux. [87]

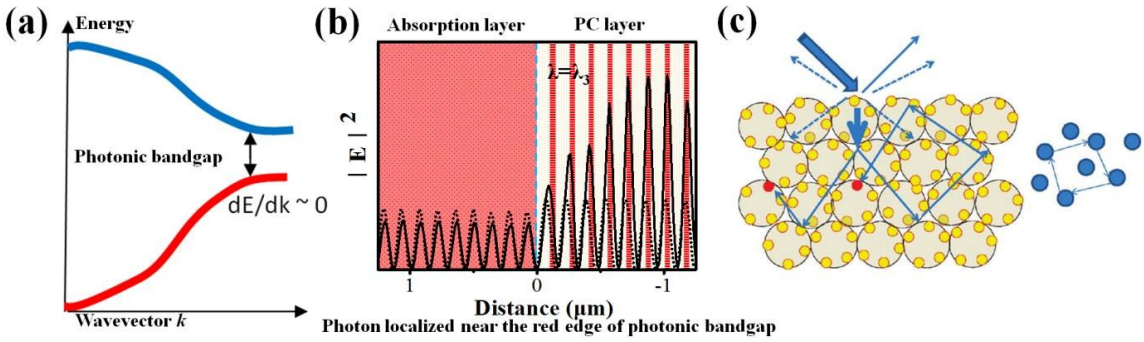


Fig. 15 (a-b) Simplified optical band structure of PC and the schematic representation of the standing wave formed in the PC for light located at the edge of the stop band. Reprinted with permission from ref. 63. Copyright (2011) John Wiley and Sons. (c) Schematic illustration of Bragg reflection, diffuse scattering and multiple internal reflection/scattering in IO PCs. Reprinted with permission from ref. 44. Copyright (2010) American Chemical Society.

Apart from the above-mentioned light trapping functionality, PCs have also been used to provide other functionalities, such as the direction-selective filter on top and intermediate layers in tandem cells.[85] To explore more functionalities of PCs for applications in sensitized solar cells, continued effort should be made to design novel PC structures and cell architectures and to understand the underlying mechanisms.

## 4 Application of PCs in sensitized solar cells

### 4.1 Liquid-state DSSCs

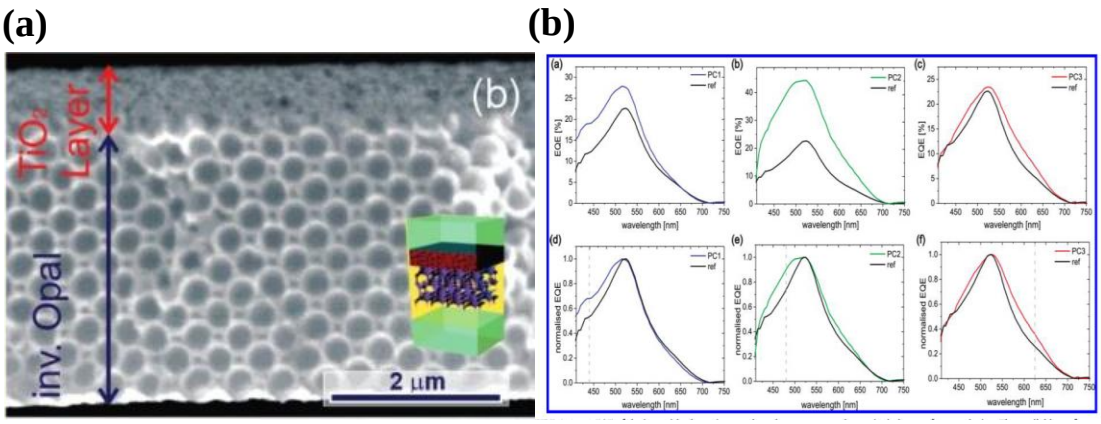


Fig. 16 (a) Morphology of the bi-layer structured photoanode. Reprinted with permission from ref. 53. Copyright (2008) American Chemical Society. (b) EQE and normalized EQE of DSSCs coupled with $TiO_2$ IO PCs of three different cavity diameters. Reprinted with permission from ref. 43. Copyright (2010) American Chemical Society. From left to right, the template diameter for fabricating IO PCs is 240, 260, and 350 nm, respectively.

As mentioned before, the successful integration of PC structure in DSSCs was first exploited by Mallouk *et al.* in 2003.[16] In their work, a 3μm thick $TiO_2$ IO PC layer was used as an additional under layer coupled to a conventional 10μm thick $TiO_2$ NP layer for DSSCs based on traditional ruthenium sensitizer (N719) and iodide/triiodide contained liquid electrolyte, resulting in photocurrent enhancement of 26%, compared with a reference cell without the PC layer. They attributed the increased absorbance in red spectral range to the slow photons at the red edge of the stop band.[16] Later, resonant modes localized in the $TiO_2$ NP layer in the stop band were thought to play the major role according to simulation result (detailed explanation described in section 3.2), which implied that the light harvesting capability and conductivity of the PC itself was not necessary, allowing flexibilities in the selection of PC (such as 1D $SiO_2/TiO_2$ PC) and the design of PC based DSSCs.[83] Subsequently, experimental work on various configurations of $TiO_2$ IO PC coupled DSSCs confirmed the formation of standing waves in the $TiO_2$ NP layer of the bi-layer structured

photoanodes (Fig. 16a), as evidenced by the increased external quantum efficiency (EQE) in the stop band region (Fig. 16b).[43] Combined with the light scattering from defects or disorders in the PC film, the PCE of DSSC was increased from 6.5% to 8.3%.[46, 53]

In conjunction with these efforts, many studies on the bi-layer photoanodes have been expanded to better the performance of the PC and consequently the devices. Hu *et al.* analyzed the influence of IO PC geometric structure and its optical properties on the photovoltaic performance of the IO PC coupled DSSCs. It was proposed that the optimized PC structure should has its stop band matched with the absorption peak of dye.[41] Modified $TiO_2$ IO structure, including $TiO_2$ quasi-IO[60] and mesoporous IO PC films[102], were also fabricated to improve the scattering effect and the surface area of the PC films. By coupling the $TiO_2$ quasi-IO layer, the PCE was increased from 3.0% to 5.7% for ~4.1μm thick $TiO_2$ NP layer and from 4.0% to 6.1% for ~10μm thick $TiO_2$ NP layer. However, the open circuit voltage ($V_{oc}$) showed a decrease after the introduction of the IO PC, as a result of the increased number of recombination sites in IO PC layers.[60] Compared to the normal $TiO_2$ IO PC, 10% higher PEC was also achieved by coupling 5 μm thick $TiO_2$ mesoporous IO PC to 10 μm thick $TiO_2$ NP layer, leading to a PEC of 6.51%.[92] An interesting work introduced by Hu *et al.* was the coupling of the IO PC structure with the plasmonic nanoparticle array, by loading Au nanoparticles inside the $TiO_2$ IO PC film.[93] As a result, increase of 60% in absorption and 41% in PCE were achieved in bi-layer DSSCs with a 6μm thick $TiO_2$ NP absorbing layer. This work demonstrated that the coupling of PC and plasmonic nanoparticles induces synergetic modulation of the incident light for resonant enhancement in light harvesting of DSSCs, which is meaningful not only in DSSC, Si, organic and quantum dot solar cells, but also in other photoelectronic devices.

$TiO_2$ IO PC structure has also been investigated as a sinlge layer photoanode for DSSCs, mainly due to its connected network for electron transport, fully connected pores for electrolyte infiltration and flexible optical design opportunities. Although the efficiency is

limited by the low surface area, several attempts involving optimizing the structure and fabrication process have been made to improve the cell performance, providing guidance and new strategies for future applications. For example, ALD technique was employed to fabricate high quality IO films and due to the high filling fraction, a PCE of 2.22% was obtained by using D149 dye and iodine based liquid electrolyte.[13, 94] It is worth noting that an interesting bi-layer IO structure was proposed by Sorge and Moon *et al.* who used a co-deposition method (mentioned in section 2.2) to obtain a PCE of 4.5%, using N535 dye and iodolyte electrolyte (Fig. 17a).[57] Post treatment on prepared $TiO_2$ IO films by $TiCl_4$ or $TiO_2$ precursor solutions to form mesoporsous $TiO_2$ film into macroporous IO networks resulted in a dual size-scale IO structure with a PEC of 4.6% and 4%, respectively (Fig. 17b).[51, 67] Higher PCEs of 6.9% and 7.23% were achieved by further modification of this dual size-scale $TiO_2$ IO structure through building twined IO films and coating with $Nb_2O_5$, respectively.[50, 95, 96]

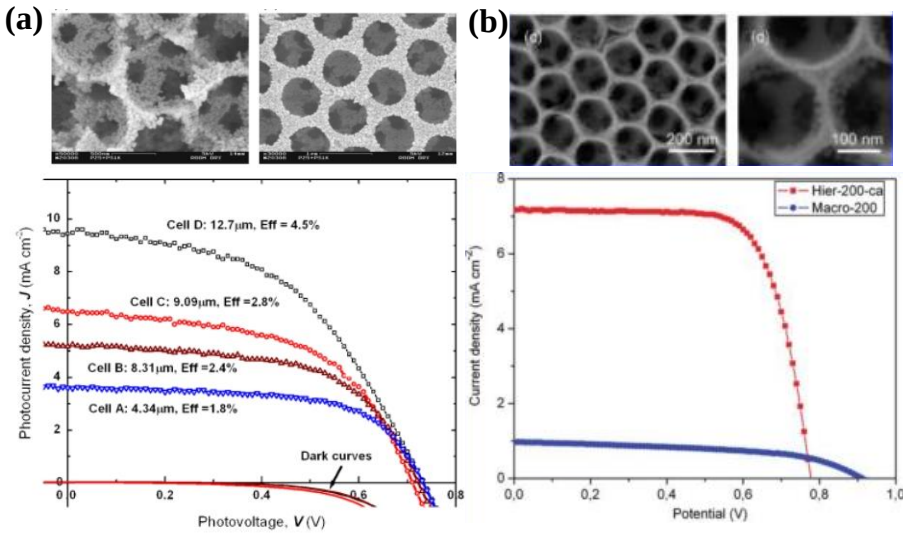


Fig. 17 Structure and *J-V* curves of DSSCs based on a dual size-scale $TiO_2$ IO structure made by (a) co-deposition and (b) post treatment. Reprinted with permission from ref. 57. Copyright (2009) John Wiley and Sons. Reprinted with permission from ref. 67. Copyright (2011) American Chemical Society.

Based on the aforementioned theoretical prediction on the possibility of using insulating or non-absorbing PC structure in bi-layer DSSCs, porous 1D multilayer PCs were introduced to replace the IO PC, attempting to avoid the disadvantages of IO PC coupled DSSCs, such as poor charge transport and high recombination of thick IO PC films and poor transparency caused by scattering of the IO PC.[32, 35, 89] Porous 1D $TiO_2/SiO_2$ PC is highly reflective within the stop band, preserving the transparency of the cell outside of the stop band (Fig. 18b and d). Its porous structure also enables electrolyte diffusion. Consequently, by coupling a ~500nm thick 1D $TiO_2/SiO_2$ PC layer, whose stop band matches the absorption peak of dye, to a 7.5μm thick $TiO_2$ NP layer, a PCE of 4.6% (increased by 18%) was achieved (Fig. 18a).[32] The PCE can be further increased by 45% if the porosity was enlarged(Fig. 18c) or if a multi-period $TiO_2/SiO_2$ PC layer (described in previous section) was integrated.[36, 89] However, incomplete penetration of electrolyte due to the alternating dense nanoparticle layers is the reason for relatively low PCEs.

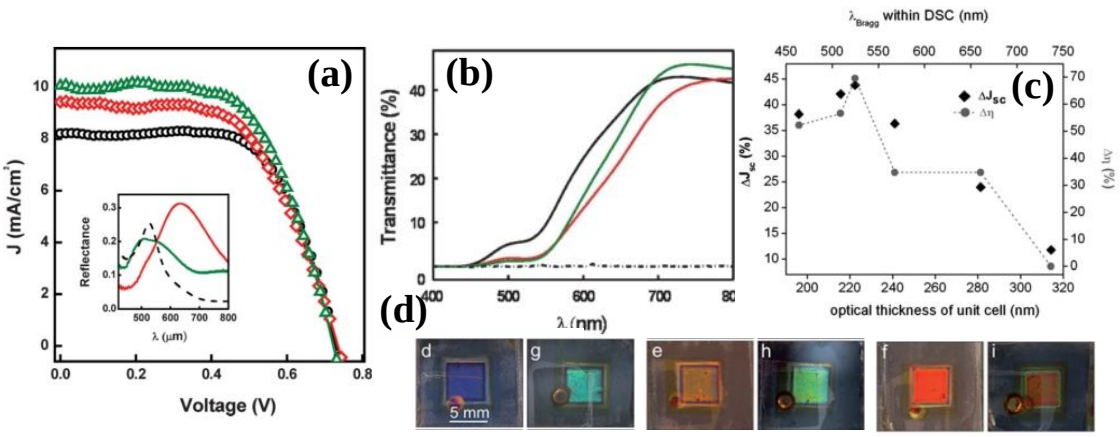


Fig. 18 (a) Photocurrent-voltage (*J*-*V*) curves and (b) transmittance spectra of DSSCs coupled with 1D $TiO_2/SiO_2$ PC. Reprinted with permission from ref. 32. Copyright (2009) John Wiley and Sons. (c) The photocurrent and PCE enhancements obtained by using highly porous 1D $TiO_2/SiO_2$ PC, and (d) photos of assembled transparent DSSCs showing different colors. Reprinted with permission from ref. 89. Copyright (2012) Royal Society of Chemistry.

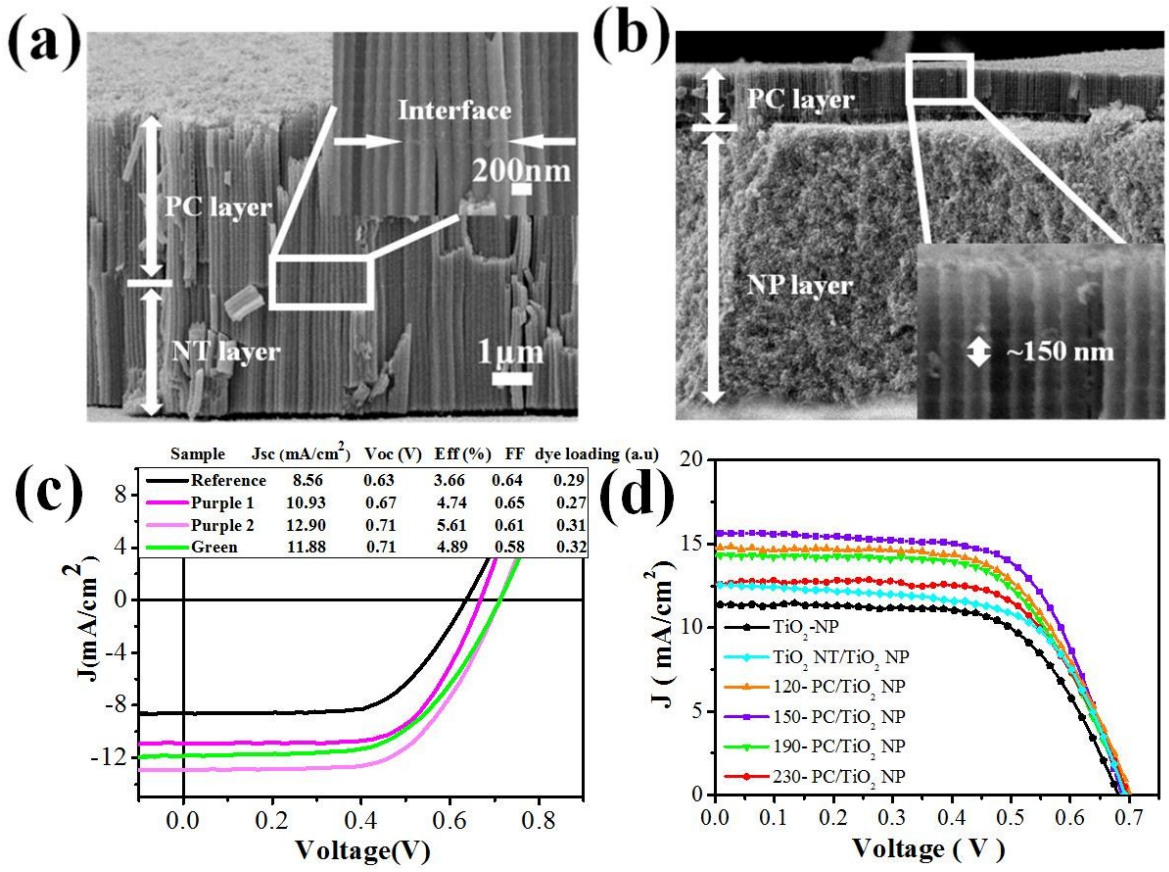


Fig. 19. (a), (b) The SEM image of two types of $TiO_2$ NT PC based photoanodes; (c), (d) The corresponding I-V curves of DSSCs coupled with the two $TiO_2$ NT PCs. Reprinted with permission from ref. 63. Copyright (2011) John Wiley and Sons. Reprinted with permission from ref. 62. Copyright (2012) Royal Society of Chemistry.

We have designed two novel architectures of $TiO_2$ NT PC-based photoanodes for DSSCs (Fig. 19a and b).[62, 63] The first one is a seamlessly coupled $TiO_2$ NT PC layer and a $TiO_2$ NT absorbing layer ($TiO_2$ NT/PC membrane) which was fabricated by a single-step anodization approach with the PC layer anodized under periodic current pulses, followed by a smooth-walled $TiO_2$ NT layer anodized under constant current. The bi-layered $TiO_2$ NT/PC based photoanode efficiently get rid of the following possible intrinsic drawbacks of 1D multilayer PC- and 3D IO PC-based photoanode:[63] (1) poor physical contact between the PC layer and the $TiO_2$ absorbing layer; (2) a nonconductive PC layer that hinders the charge

transport (leading to poor fill factor); (3) electrolyte being easily clogged at the interface; (4) the photonic bandgap being impossible to be continuously tuned for the optimization of light harvesting; (5) the thickness of the absorbing layer having to be very thin to satisfy the stringent requirement on interface flatness. When the stop band of the $TiO_2$ NT PC best matches that of dye absorption peak, the DSSCs equipped with this bi-layer structure showed a significantly enhanced PCE (5.61%), an increase of over 50% compared with the cells without a PC layer (3.66%)(Fig. 19c).

However, the PCE is still low as compared with the state-of-the-art nanoparticle-based counterpart due to the relatively lower surface area of NT-based photoanode. A new design was proposed by replacing the $TiO_2$ NT absorbing layer with a thick $TiO_2$ nanoparticle layer to enhance the surface area for dye absorption (Fig. 19b). To preserve the transparency of DSSC, only a thin $TiO_2$ NT PC layer was coupled to the photoanode.[62] The combined effects of PC and light-scattering yield the maximum enhancement in PCE (39.5%) when the stop band of $TiO_2$ NT PC best matches the dye (N719) absorption peak, leading to a high PCE of 6.96% of the $TiO_2$ NT PC-based DSSCs(Fig. 19d).

There are also several pieces of work on PC coupled counter eletrode, which reflects light in the selective spectrum range back to the absorbing layer. Cho *et al.* attached a 1D multilayer PC consisting of alternating polymeric films of different refractive indices to the back side of the counter electrode, leading to 10% higher efficiency than the reference cell without the PC outside layer.[97] Recently, a 1D organic-inorganic multilayer PC, built up of photo-crosslinkable PS-b-P4VP (denoted as S4VP) and PS-b-PEO (denoted as SEO) containing $TiO_2$, has also been fabricated on the opposite side of platinum sputtered FTO glass. Compared with reference devices, an enhancement of up to 11% of the DSSCs containing 1D S4VP-SEO/$TiO_2$ multilayer PC was achieved.[98] More interestingly, the use of conductive PC structure deposited on FTO or ITO to replace the Pt-coated FTO counter electrode, such as IO carbons and 1D multilayer PC with alternating $SiO_2$ NP layer and

sputtered ITO layer, has also been demonstrated to increase the efficiency, taking advantages of the fast electron transport in the highly interconnected structure and selective reflection from the PC.[39, 99]

### 4.2 Solid-state DSSCs

Although the state-of-the-art DSSCs that use liquid electrolyte still show the highest PCE, solid-state DSSCs (ss-DSSCs) using solidified or quasi-solid-state polymer electrolyte and solid-state hole transport materials have attracted a lot of interest in an attempt to replace the liquit electrolyte, which is corrosive, volatile, photoreactive and instable. Early attempt to use 3D IO PC in ss-DSSCs was based on the concept of utilizing large interconnected pores for efficient infiltration of solid-state electrolyte and at the same time making use of the multiple internal scattering of 3D IO PC.[49, 55, 58] In many cases, the 3D IO PC film was assembled as a single layer photoanode. However, the efficiency was low. Hwang *et al.* constructed double-layered ss-DSSC consisting of a conventional $TiO_2$ NP layer and a $TiO_2$ IO PC underlayer.[40] After loading of N719 dye and infiltrating ($P_{1,4}I$)-doped succinonitrile solid electrolyte, a high PCE of 8.2% was obtained when a 4μm thick $TiO_2$ NP layer was coupld to a 20μm thick $TiO_2$ IO PC layer, about 50% higer than that of the ss-DSSC with only a 8μm thick $TiO_2$ NP layer. They also attributed the efficiency increase to a combination of the effects, such as, back reflection in the stop band of the IO PC, multiple scattering from the cracks in the IO films and the resonant modes confined in the $TiO_2$ NP layer, similar to the case of 3D IO PC in liquid-state DSSCs.

The application of 1D $SiO_2/TiO_2$ PC in ss-DSSCs, as an underlayer in photoanode or a back layer attached to counter electrode, was also proposed by Kim *et al.*[37, 38] An interesting three-layer ss-DSSCs, composed of a 500nm thick organized mesoporous $TiO_2$ layer on the top, a 10μm thick $TiO_2$ NP layer in the middle and a 2μm thick porous 1D $SiO_2/TiO_2$ PC layer at the bottom (Fig. 20a-b), were constructed layer by layer through sol-gel,

doctor-blade, and spin-coating methods.[38] The solid-state polymerized ionic liquid (PIL) electrolyte was added and deeply infiltrated by three steps: (1) dissolving PIL in acetonitrile, (2) casting the PIL solution on the photoelectrode, and (3) superimposing and pressing with a counter electrode to slow down the evaporation of the solvent. In this hetero-structured photoanode, the top mesoporous $TiO_2$ layer deposited on the FTO glass increases the visible light transmittance by decreasing the effective roughness of the FTO glass and also facilitates the easy electron transport to the FTO (Fig. 20c). Simultaneously, the 1D $SiO_2/TiO_2$ PC layer at the bottom offers spectral reflection at the wavelengths near the dye absorption peak and scattering effect from the thick dielectric layers in the PC (Fig. 20d). As a result, the short circuit current ($J_{sc}$) of the cell was increased from 13.7mA·cm$^{-2}$ to 18.3 mA·cm$^{-2}$, with enhanced IPCE in the whole visible range, leading to the final PCE of 6.6%. The same value of PCE could also be obtained after moving the 1D $SiO_2/TiO_2$ PC layer to the back side of the counter electrode.[37]

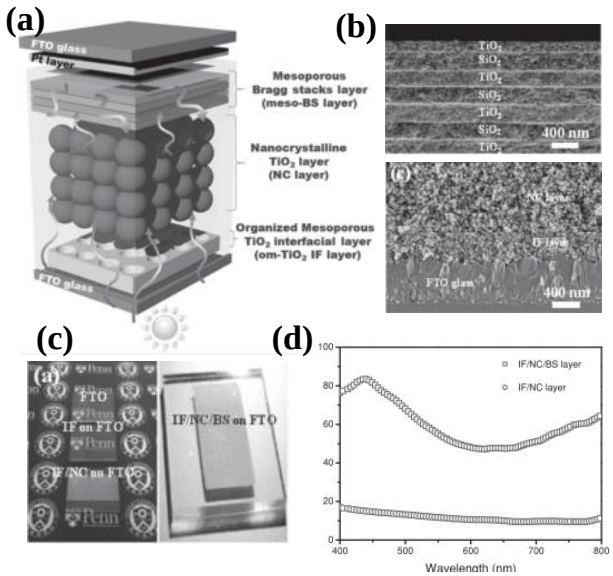


Fig. 20 Structure and the performance of the three-layer photoanode and the corresponding ss-DSSCs: (a) Structure sketch of the device, (b) SEM images of the photoanode, (c) photographs of the device at different stages, (d) Reflectance spectra. Reprinted with permission from ref. 38. Copyright (2013) John Wiley and Sons.

A novel 1D $TiO_2$/$TiO_2$ PC, which comprises of organized mesoporous $TiO_2$ layers of high (2.0) and low (1.7) refractive indices, was recently constructed via a sol-gel process using two copolymer templates with different graft ratios. With optimized structure of the PC-based photoanode, consisting of 400nm thick organized mesoporous $TiO_2$ interfacial layer, 7μm thick nanocrystal $TiO_2$, and 1.2μm thick 1D $TiO_2$/$TiO_2$ PC, an excellent efficiency of 7.5% was achieved in the polymerized ionic liquid based ss-DSSC, which is much higher than that of nanocrystal $TiO_2$ photoanode (3.5%).[100]

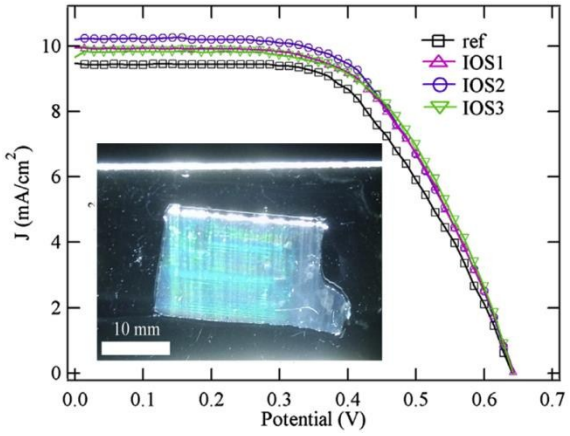


Fig. 21 Typical I-V curves for the DSSCs composed of different gel electrolyte IO PCs. The gel electrolyte IO PCs possess photonic band gaps around 530 nm (IOS1), 690 nm (IOS2), and 770 nm (IOS3). The inset is a photograph of a typical gel electrolyte IO PC. Reprinted with permission from ref. 101. Copyright (2015) Elsevier.

Very recently, by using $SiO_2$ opal films as templates and subsequent template etching, a polymer gel electrolyte with IO structure (gel electrolyte IO PC) was first applied in ss-DSSCs (Fig. 21a).[101] By tailoring light propagation in the ss-DSSCs, a maximum average PCE of 3.85% was achieved for the gel electrolyte IO PC with a photonic bandgap around 690 nm, which was about 10% higher than that of the reference gel electrolyte (3.48%)(Fig. 21b). The gel electrolyte IO PC gives rise to random back scattering and back reflection of photons and thus enhances PCE of the ss-DSSCs. In addition to the optical effects of the IO

structure, other main factors affecting the PCE of the device are the diffusion resistance of the electrolyte and the interfacial charge transport resistance.[102, 103] A lower Warburg impedance of the gel electrolyte also contributes to the PCE enhancement of an IO PC coupled device.[102] This study offers new strategy and new insight to the coupling of PC to a solar cell for light management.

### 4.3 Quantum-dot sensitized solar cells

Quantum-dots (QDs) used in solar cells are usually inorganic nano-sized semiconductor particles, whose bandgaps and relevent optical properties are size-dependent. In addition to their unique tunable bandgap, which enables tunable absoption spectrum for device performance optimization, QDs possess the advantages of photostability, high extinction coefficients, large intrinsic dipole moments and low cost. Thus, QD-sensitized solar cells (QDSSCs), using QDs as the light harvesting materials in lieu of organic dyes, have become a popular research topic as the third generation solar cells in recent years. Moreover, multiple exciton generation phenomenon (exciting multiple electron-hole pairs per photon) has been demonstrated in QDs, leading to a predicted PCE up to 44% for QDSSCs.[104] Actually, the construction and operation mechanism of QDSSCs is very similar to that of DSSCs, where the QDs play the role of dye molecules to generate photo-excited electrons, which are subsequently injected into a nanostructured semiconductor (typically $TiO_2$) photoanode. However, the different fabrication processes and properties of QDs give rise to new requirments on the materials, structures and configurations used in the QDSSCs. For example, the commonly used mesoporous $TiO_2$ NP (szie ~ 10-15nm) photoanodes with large surface area, are not suitable for QDSSCs, due to the difficulties encountered in the loading of nanosized QDs and also the electrolyte infiltration into the films. In addition, the high extinction coefficient of QDs lowers the requirement on large surface area of the photoanode. Thus, $TiO_2$ IO PC structure was proposed to be used as single layer photoanode for QDSSCs

due to its large interconnected pores, interconnected network for electron transport and great potential for optical design.

Diguna *et al.* contructed CdSe QDSSCs by chemical deposition on $TiO_2$ IO films made by templates of different diamters of 309 nm and 394 nm.[47] Good infiltration of the Cd/Se precursors and the electrolyte into the $TiO_2$ IO structure contributed to the relatively high PCE of 2.7% for QDSSCs. Moreover, it was also demonstrated that $TiO_2$ IO with larger pores gave rise to higher fill factor (*FF*) and PEC than those of smaller pores with larger surface area, which showed the difference, as described above, between QDSSCs and DSSCs.

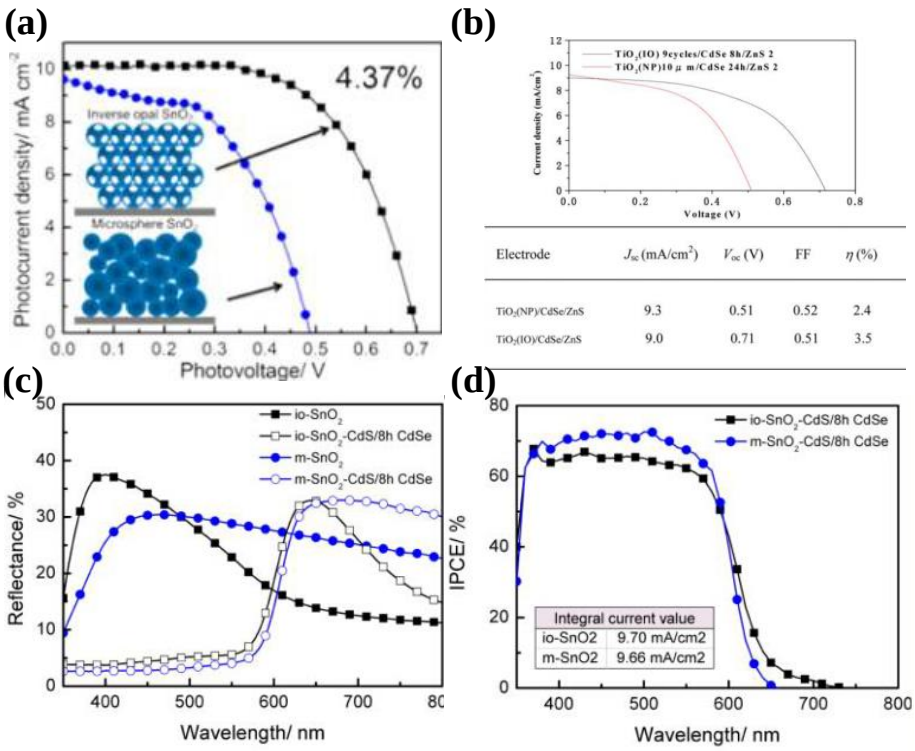


Fig. 22 (a-b) *J-V* curves and photovoltaic performance of QDSSCs based on 3D IO single layer photoanodes made of (a) $SnO_2$ and (b) $TiO_2$. Reprinted with permission from ref. 54 and 105. Copyright (2014 and 2012) American Chemical Society. (c) The reflectance spetra of $SnO_2$ IO films before and after QD deposition. Reprinted with permission from ref. 54. Copyright (2014) American Chemical Society. (d) IPCE of the QDSSCs using $SnO_2$ IO and mircosphere single layer photoanodes. Reprinted with permission from ref. 54. Copyright (2014) American Chemical Society.

Recently, Toyoda found highly increased $V_{oc}$ in CdS/CdSe QDSSCs made by chemical bath deposition (CBD) method based on both $TiO_2$ and $SnO_2$ IO films, as compared with the NP or mircosphere based cells (Fig. 22a-b).[54, 105] Red shift of the reflection peak after the depositon of QDs (CdS and CdSe) was also observed (Fig. 22c), which was caused by the increased effective refractive index, and led to a slightly enhaneced IPCE in the red wavelength range (≥600nm, Fig. 22d).[54] Due to the less amount of deposited QDs and the front reflection of the PC structure, the IPCE values over the whole spectrum and the $J_{sc}$ of the $SnO_2$ IO PC based QDSSCs were still similar to the mircosphere based cells, but smaller than the conventional NP based ones. Nonetheless, higher efficiencies of 3.5% ($TiO_2$ IO) and 4.37% ($SnO_2$ IO) could be achieved as a result of the remarkably improved $V_{oc}$ (Fig. 22a-b), which was attributed to the reduced charge recombination rate in the IO structure.

Although enhanced PCE values have been obtained in the above mentioned work, photonic effects of the IO PC structure in QDSSCs and how to fully utilize its optical perporties were not thoroughly studied. In constrast, Halaoui *et al.*demonstrated noticeable enhancements in the photocurrent efficiency caused by optical effects of the $TiO_2$ IO PC film in a 3-electrode quartz photoelectrochemical cell system using CdS or CdSe QDs.[44, 106] Fig. 23a displays the relationship of the absorption edges of the CdS QDs and the stop band peaks of the IO PC films. By using CdS QDs with the absorption edge at 410nm, a much higher blue-edge gain of IPCE was obtained in $TiO_2$ IO PC with stop band at 450nm (4.7±2.6, measured at 420nm), compared with the red-edge gain of 1.4-1.8 measured at the same wavelength using $TiO_2$ IO PC with stop band at 390nm (Fig. 23b-c). The observed larger blue-edge enhacement factor than the red-edge one in IO PC coupled QDSSCs implies that the photon licalization mechanism may be different from the situation in DSSCs.[44] Novel design and further optimization of the PC configurations are highly desirable for future application of PC in QDSSCs.

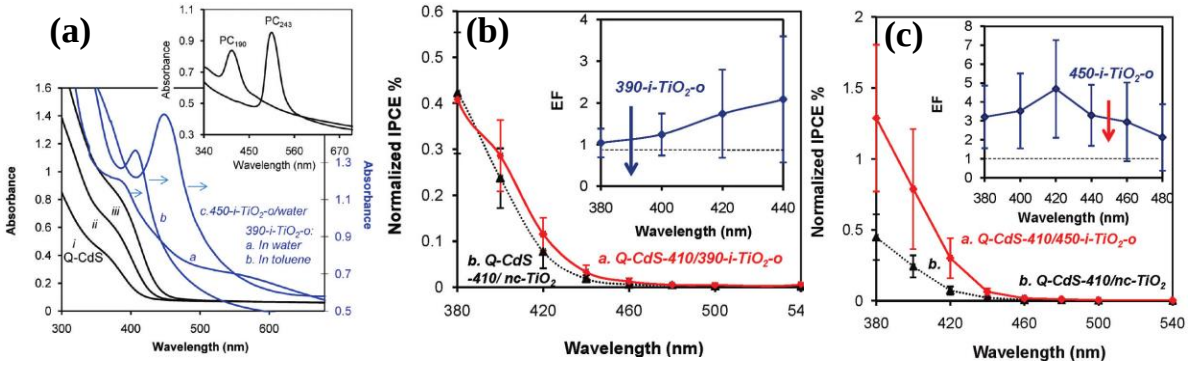


Fig. 23 (a) Absorption spectra of CdS QD solution and the stop band position of IO PCs. (b-c) Average normalized IPCE and the gain of QDSSCs based on $TiO_2$ IO PC with stop band at (b) 390 nm and (c) 450 nm. The enhancement factor (EF, ratio of normalized IPCE of $TiO_2$ IO PC to that of nanocrystalline $TiO_2$) is shown in the inset. Reprinted with permission from ref. 44. Copyright (2010) American Chemical Society.

As early as 2012, Toyoda *et al.* pointed out that the morphology of the $TiO_2$ photoanode was one of the main factors for satisfactory assembly of QDSSCs with improved PCE.[105] It is believed that the breakthrough in PCE for next-generation QDSSCs will come from two types of photoanode morphologies, namely, (a) $TiO_2$ NT photoanode and (b) $TiO_2$ IO PC photoanode. The advantage of employing $TiO_2$ NT as the photoanode is its low recombination probability of photogenerated electrons and holes. While the $TiO_2$ IO PC photoanode is advantageous in light harvesting. Fortunately, $TiO_2$ NT PC owns both of the characteristics at the same time and is therefore worthy of exploration.

### 4.4 Perovskite solar cells

Studies on perovskite solar cells have recently emerged from the field of DSSCs by employing organic-inorganic perovskite materials as absorbers.[107, 108] There have been many breakthroughs and rapid evolution in the field of emerging perovskite solar cells, with the realization of both high efficiency and low cost.[109-112]

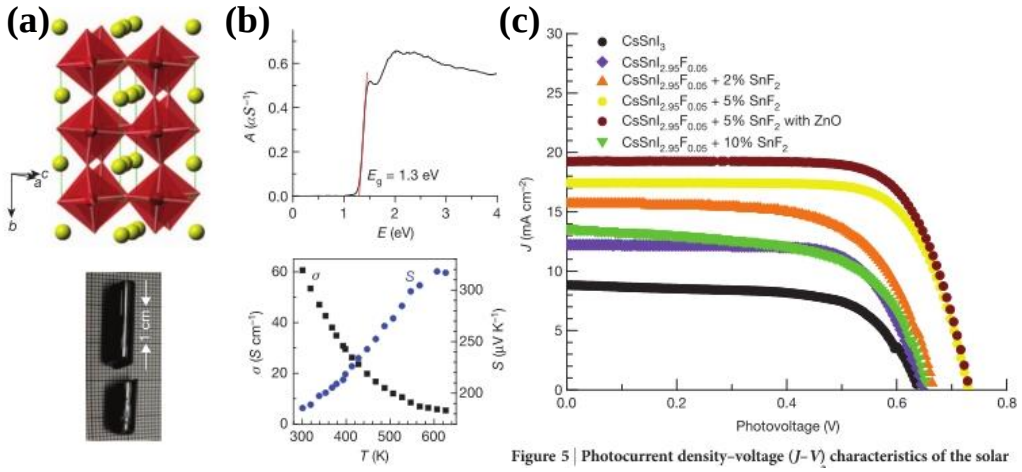


Figure 5 | Photocurrent density–voltage ($J$–$V$) characteristics of the solar

Fig. 24 (a) Perovskite crystal structure and photograph, and (b) optical absorptance and electrical conductivity of $CsSnI_3$. (c) *J-V* curves of the DSSCs based on $CsSnI_3$ ss-electrolyte. To improve the PCE, ZnO 3D IO PC was used. Reprinted with permission from ref. 6. Copyright (2012) American Association for the Advancement of Science.

In 2012, the work by Kanatzidis *et al*. triggered the research on perovskite sensitized solar cells.[6] In this work, an inorganic perovskite, $CsSnI_3$, was first used as solid-state hole transport material (HTM) to replace the liquid electrolyte (Fig. 24a). Due to its p-type nature, direct bandgap of 1.3eV, high hole mobility, and suitable conduction band position (3.62 eV), remarkable high PCE of 9.28% was achieved for N719 sensitized ss-DSSCs after doping $CsSnI_3$ with F and $SnF_2$ (Fig. 24b). The PCE was further improved to 10.2% by coupling two layers of ZnO 3D IO PC to the counter electrode (Fig. 24c). The double layered ZnO IO PC films were frabricated by ALD using PS templates and diethyl zinc and water as precursors, which have also been succesfully utilized in tranditional liquid-state DSSCs to obtain a PCE of 12.5%, 15% higher than that of the one without ZnO IO PC.[6, 86] This work has boosted intense research interest on perovskite material based solar cells and, nowadays, extremely high PCE, far beyond that of DSSCs, has been achieved in perovskite solar cells.[109, 110, 113-116]

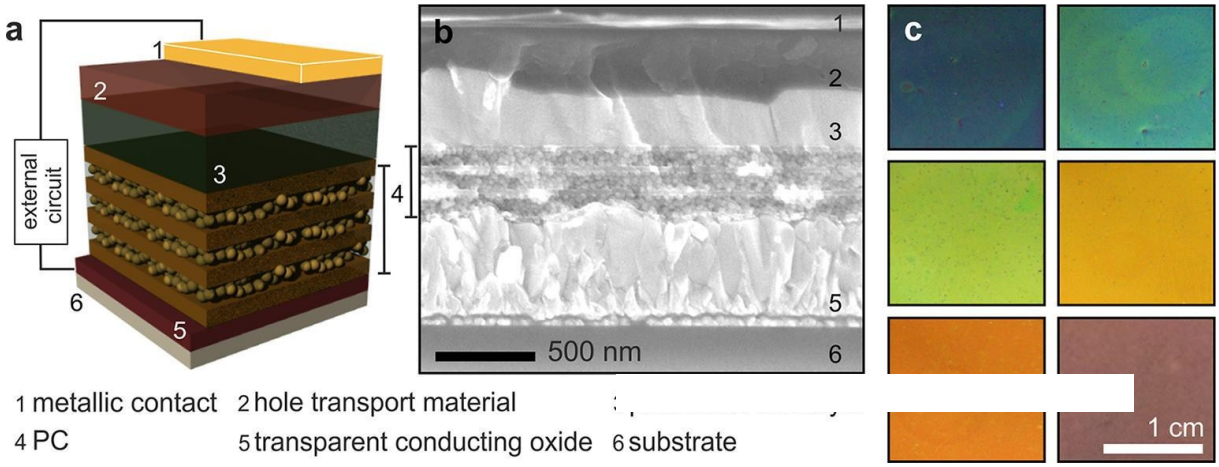


Fig. 25 (a) Scheme of a PC-based perovskite solar cell. (b) Cross-section SEM image of a PC-based perovskite solar cell. (c) Colors (from blue to red) displayed by devices integrated with different PCs. Reprinted with permission from ref. 117. Copyright (2015) American Chemical Society.

Due to the very high extinction coefficient of the perovskite and the excellent light absorption in almost the whole visible range, perovskite solar cell can easily achieve a PCE far beyond that of a DSSC, which makes the use of PC no longer necessary in a perovskite solar cell. Nevertheless, for practical applications, factors other than efficiency should be considered. For example, the building integrated photovoltaics should usually be aesthetically versatile, being both colorful and semitransparent. In order to achieve efficient and color-tunable perovskite solar cells, Miguez and Snaith integrated the cells with 1D $TiO_2/SiO_2$ PC (Fig. 25a).[117] By optimizing the microstructures of the $TiO_2$ and $SiO_2$ layers to achieve a balance between minimization of the PC layer thickness and preservation of its high reflectance (Fig. 25b), the fabricated devices show intense colors across the visible spectrum, from blue to red (Fig. 25c). Under back-side illumination, the best PCE of blue, blue-green, green, orange and red cells is 8.8%, 7.0%, 6.7%, 6.6% and 4.5%, respectively, indicating the great potential for making efficient perovskite solar cells with vivid and tunable colors. It can

be seen from this example that the coupling of PC will render perovskite solar cells more functionalities for wider applications.

## 5 Summary and outlook

In summary, recent developments of photonic crystals for sensitized solar cells, including their fabrication methods, functionalities in the devices and the photovoltaic characteristics of PC based sensitized solar cells, were reviewed. Compared with other geometric optics components for solar cell applications, such as metallic mirror and large particle scattering layer, PCs possess the advantages of (1) selective spectral response which maintains high efficiency and transparency of the devices at the same time, (2) porous structure that allows the infiltration of electrolyte, (3) an incident angle dependent Bragg position to enable the compensation of cosine loss under titled light, and (4) many other functionalities that are specific to the type of PC. Some successful examples of the utilization of 1D multilayer PC, 3D IO PC, and $TiO_2$ NT PC in sensitized solar cells (including liquid-state DSSCs, solid-state DSSCs, quantum-dot sensitized solar cells, and perovskite solar cells), have been highlighted in this review.

As an alternative, integrating plasmonic metallic nanoparticles into sensitized solar cells, which are characterized by strong interaction with resonant photons through the excitation of surface plasmon resonance, is another option to manage photons for enhancing the PCE of the solar cells.[118,119] Nevertheless, in most of the early work, the photoanodes were fabricated by incorporating Ag and Au nanocrystals into $TiO_2$ matrix using chemical methods,[120-123] and only improved light absorption was observed without any improvement in PCE of the liquid-state DSSCs. This phenomenon was attributed to the corrosion of the metal nanocrystals by liquid electrolytes, as well as the recombination and back reaction of photo-generated charge carriers, leading to decreased PCE and instability of DSSCs. A general strategy to overcome the above-mentioned problems is to coat a thin $SiO_2$ or $TiO_2$ layer on the

metal nanocrystals.[124, 125] For example, the PCE of an N719 DSSC (9.3%) was increased to 10.2% and 9.8% with the incorporation of $Au@SiO_2$ and $Au@TiO_2$ NPs, respectively.[125] However, the percentage enhancement of PCE is still far below the theoretical predicted value. It seems that, at present, the use of plasmons in sensitized solar cells is no better than its PC counterpart.[126] But we believe that there are still plenty of rooms in coupling PC and plasmons for enhanced performance of sensitized solar cells.

As for PC itself, it is difficult to say which type of PC is the best. Each type of PC has its own advantages and disadvantages. The selection of the correct type of PC depends on the application purpose. Tab. 2 summarizes the characteristics of typical PCs-based sensitized solar cells. It should be noted that, although large improvements continue to be made in this specific area, which are benefitted from the progress of the PC fabrication techniques as well as the design and optimization of structural configurations in these solar cells, it is still a long way for PC-coupled sensitized solar cells to be commercialized.

The fruitful future of PCs in the applications of sensitized solar cells and other types of irradiance sensitive photonic devices relies on (1) the design of novel PC structures with the help of powerful computer simulations, (2) the development of novel fabrication techniques for large scale and mass production of PCs, (3) deepened understanding on the light propagation and material-light interaction in devices, (4) exploration of new functionalities of PC-coupled devices, and (5) the study of novel plasmonic enhanced PC effect in devices. The bright future of this exciting area also relies on the close multidisciplinary collaboration among physicists, chemists, and material scientists.

Table 2 Comparison of the characteristics of typical PC-coupled sensitized solar cells.

| Type of PCs | Position | Methods | $\eta_1$ (%) | $\eta_2$ (%) | ref |
|---|---|---|---|---|---|
| Liquid-state DSSCs | | | | | |
| 1D $SiO_2/TiO_2$ PC | Photoanode | Spin-coating | 6.8% | 7.0 % | [35] |
| 1D $SiO_2/TiO_2$ PC | Counter electrode | Spin-coating | 7.6% | 7.9% | [39] |
| 1D S4VP /SEO-$TiO_2$ PC | Backside of counter electrode | Spin-coating | % | % | [98] |
| 3D IO $TiO_2$ PC | Backside of counter electrode | Templated-assistant | 10.9% | 12.5% | [87] |
| 3D IO $TiO_2$ PC | Photoanode | Templated-assistant | 2.0% | 1.8% | [43] |
| 3D IO $TiO_2$ PC | Photoanode | Templated-assistant | 3.0% | 5.7% | [60] |
| $TiO_2$ NT PC | Photoanode | Anodization | 3.7% | 5.6% | [63] |
| $TiO_2$ NT PC | Photoanode | Anodization | 5.0% | 7.0% | [62] |
| $TiO_2$ NT APC | Photoanode | Anodization | 6.2% | 7.9% | [68] |
| Solid-state DSSCs | | | | | |
| 1D $TiO_2/TiO_2$ PC | Photoanode | Spin-coating | 3.5% | 7.5% | [100] |
| 1D $SiO_2/TiO_2$ PC | Backside of counter electrode | Spin-coating | 3.5% | 6.4% | [38] |
| 1D $SiO_2/TiO_2$ PC | Counter electrode | Spin-coating | 5.4% | 6.6% | [37] |
| 3D IO $TiO_2$ PC | Photoanode | Templated-assistant | 5.5% | 7.2% | [40] |
| 3D IO gel electrolyte | Electrolyte | Templated-assistant | 3.5% | 3.9% | [101] |
| QDSSCs | | | | | |
| 3D IO $SnO_2$ PC | Photoanode | Templated-assistant | 2.4% | 4.4% | [54] |
| 3D IO $TiO_2$ PC | Photoanode | Templated-assistant | 2.4% | 3.5% | [105] |
| Perovskite solar cells | | | | | |
| 3D IO ZnO PC | Counter electrode | Templated-assistant | 9.28% | 10.2% | [6] |
| 1D $SiO_2/TiO_2$ PC | Interlayer | Spin-coating | 10.5% | 8.8% | [117] |

Note: $\eta_1$ PCE of solar cells without PC, $\eta_2$ PCE of solar cells with PC.

## Acknowledgements

This work is supported by the Research Grants Council of the Hong Kong Special Administrative Region, China (Project Nos. PolyU5163/12E, PolyU5159/13E and PolyU152057/14E). KYX is grateful for the financial support from the National Natural Science Foundation of China (No.51302219).

**Dr. Keyu Xie** received his Ph.D. degree in 2012 from Central South University, China. From 2010 to 2013, he stayed in Hong Kong Polytechnic University as a Research Assistant and Postdoctoral Research Associate successively. He is currently an Associate Professor at the State Key Laboratory of Solidification Processing and the Center for Nano Energy Materials in Northwestern Polytechnic University, China. His research interests include nano-materials and their application in energy storage and conversion devices, such as rechargeable batteries, supercapacitors and solar cells.

**Dr. Min Guo** received her Ph.D. degree in 2015 from the Hong Kong Polytechnic University. She is currently a lecturer at the School of Materials Science and Engineering and the State Key Laboratory of Solidification Processing in Northwestern Polytechnic University, China. Her research interests include nanomaterials and nanostructures for energy conversion, and high-temperature materials.

**Dr. Haitao Huang** received his Ph.D in Materials Science from Nanyang Technological University, Singapore in 2000. He is currently the Associate Professor in the Department of Applied Physics, the Hong Kong Polytechnic University. He has published over 160 refereed journal papers on energy materials (supercapacitors, lithium-ion batteries and dye-sensitized solar cells) and ferroelectric materials. He is currently on the editorial board of *Scientific Reports* and the advisory board of *Journal of Materials Chemistry C*.

## References

[1] P. H. J. Conti, International Energy Outlook 2011, the U.S. Energy Information Administration (EIA), (2011).

[2] K. Xie and B. Wei, *Adv. Mater.*, 2014, **26**, 3592-3617.

[3] B. Dunn, H. Kamath, and J. M. Tarascon, *Science*, 2011, **334**, 928-935.

[4] J. Goldemberg, *Science*, 2007, **315**, 808-810.

[5] S. Rühle, M. Shalom and A. Zaban, *ChemPhysChem*, 2010, **11**, 2290-2304.

[6] I. Chung, B. Lee, J. He, R. P. Chang and M. G. Kanatzidis, *Nature*, 2012, **485**, 486-489.

[7] M. Yu, Y. Z. Long, B. Sun and Z. Fan, *Nanoscale*, 2012, **4**, 2783-2796.

[8] A. Polman and H. A. Atwater, *Nat. Mater.*, 2012, **11**, 174-177.

[9] M. Graetzel, R. A. J. Janssen, D. B. Mitzi and E. H. Sargent, *Nature*, 2012, **488**, 304-312.

[10] S. B. Mallick, N. P. Sergeant, M. Agrawal, J.-Y. Lee and P. Peumans, *MRS Bull.*, 2011, **36**, 453-460.

[11] K. Vynck, M. Burresi, F. Riboli and D. S. Wiersma, *Nat. Mater.*, 2012, **11**, 1017-1022.

[12] A. Kay and M. Grätzel, *Sol. Energy Mater. Sol. Cells*, 1996, **44**, 99-117.

[13] W. Hou, P. Pavaskar, Z. Liu, J. Theiss, M. Aykol and S. B. Cronin, *Energy Environ. Sci.*, 2011, **4**, 4650-4655.

[14] Q. Zhang, T. P. Chou, B. Russo, S. A. Jenekhe and G. Cao, *Angew. Chem. Int. Ed.*, 2008, **120**, 2436-2440.

[15] E. T. Yu and J. van de Lagemaat, *MRS Bull.*, 2011, **36**, 424-428.

[16] S. Nishimura, N. Abrams, B. A. Lewis, L. I. Halaoui, T. E. Mallouk, K. D. Benkstein, J. van de Lagemaat and A. J. Frank, *J. Am. Chem. Soc.*, 2003, **125**, 6306-6310.

[17] P. Bermel, C. Luo, L. Zeng, L. C. Kimerling and J. D. Joannopoulos, *Opt. Express*, 2007, **15**, 16986-17000.

[18] P. G. O'Brien, N. P. Kherani, A. Chutinan, G. A. Ozin, S. John and S. Zukotynski, *Adv. Mater.*, 2008, **20**, 1577-1582.

[19] R. B. Wehrspohn and J. Üpping, *J. Optics*, 2012, **14**, 024003.

[20] M. A. Green, *Prog. Photovoltaics: Res. Applications*, 2009, **17**, 183-189.

[21] L. Kranz, S. Buecheler and A. N. Tiwari, *Sol. Energy Mater. Sol. Cells*, 2013, **119**, 278-280.

[22] J. Ge and Y. Yin, *Angew. Chem. Int. Ed.*, 2011, **50**, 1492-1522.

[23] R. V. Nair and R. Vijaya, *Prog. Quant. Elect.*, 2010, **34**, 89-134.

[24] C. Fenzl, T. Hirsch and O. S. Wolfbeis, *Angew. Chem. Int. Ed.*, 2014, **53**, 3318-3335.

[25] S. Furumi, *Polym. J.*, 2013, **45**, 579-593.

[26] E. Yablonovitch, *Phys. Rev. Lett.*, 1987, **58**, 2059-2062.

[27] S. John, *Phys. Rev. Lett.*, 1987, **58**, 2486-2489.

[28] G. von Freymann, V. Kitaev, B. V. Lotsch and G. A. Ozin, *Chem. Soc. Rev.*, 2013, **42**, 2528-2554.

[29] A. Stein, B. E. Wilson and S. G. Rudisill, *Chem. Soc. Rev.*, 2013, **42**, 2763-2803.

[30] J. F. G.-Lopez, M. Ibisate, R. Sapienza, L. S. F.-Perez, A. Blanco and C. Lopez, *Adv. Mater.*, 2011, **23**, 30-69.

[31] J. H. Moon and S. Yang, *Chem. Rev.*, 2010, **110**, 547-574.

[32] S. Colodrero, A. Mihi, L. Häggman, M. Ocaña, G. Boschloo, A. Hagfeldt and H. Míguez, *Adv. Mater.*, 2009, **21**, 764-770.

[33] A. Mihi, H. Míguez, I. Rodríguez, S. Rubio and F. Meseguer, *Phys. Rev. B*, 2005, **71**, 125131.

[34] F. García-Santamaría, E. Nelson and P. Braun, *Phys. Rev. B*, 2007, **76**, 075132.

[35] S. Colodrero, A. Forneli, C. L.-López, L. Pellejà, H. Míguez and E. Palomares, *Adv. Funct. Mater.*, 2012, **22**, 1303-1310.

[36] C. L.-Lopez, S. Colodrero and H. Miguez, *Phys. Chem. Chem. Phys.*, 2014, **16**, 663-668.

[37] J. T. Park, J. H. Prosser, D. J. Kim, J. H. Kim and D. Lee, *ChemSusChem*, 2013, **6**, 856-864.

[38] J. T. Park, J. H. Prosser, S. H. Ahn, S. J. Kim, J. H. Kim and D. Lee, *Adv. Funct. Mater.*, 2013, **23**, 2193-2200.

[39] L. P. Heiniger, P. G. O'Brien, N. Soheilnia, Y. Yang, N. P. Kherani, M. Gratzel, G. A. Ozin and N. Tetreault, *Adv. Mater.*, 2013, **25**, 5734-5741.

[40] D.-K. Hwang, B. Lee and D.-H. Kim, *RSC Adv.*, 2013, **3**, 3017-3023.

[41] H. Li, Q. Tang, F. Cai, X. Hu, H. Lu, Y. Yan, W. Hong and B. Zhao, *Sol. Energy*, 2012, **86**, 3430-3437.

[42] A. Mihi, C. Zhang and P. V. Braun, *Angew. Chem. In. Ed.*, 2011, **50**, 5712-5715.

[43] S. Guldin, S. Hüttner, M. Kolle, M. E. Welland, P. M.-Buschbaum, R. H. Friend, U. Steiner and N. Tétreault, *Nano Lett.*, 2010, **10**, 2303-2309.

[44] M. El Harakeh and L. Halaoui, *J. Phys. Chem. C*, 2010, **114**, 2806-2813.

[45] C.-H. Yip, Y.-M. Chiang and C.-C. Wong, *J. Phys. Chem. C*, 2008, **112**, 8735-8740.

[46] S.-H. A. Lee, N. M. Abrams, P. G. Hoertz, G. D. Barber, L. I. Halaoui and T. E. Mallouk, *J. Phys. Chem. B*, 2008, **112**, 14415-14421.

[47] L. J. Diguna, Q. Shen, J. Kobayashi and T. Toyoda, *Appl. Phys. Lett.*, 2007, **91**, 023116.

[48] L. I. Halaoui, N. M. Abrams and T. Mallouk, *J. Phys. Chem. B*, 2005, **109**, 6334-6342.

[49] P. R. Somani, C. Dionigi, M. Murgia, D. Palles, P. Nozar and G. Ruani, *Sol. Energy Mater. Sol. Cells*, 2005, **87**, 513-519.

[50] H.-N. Kim and J. H. Moon, *Curr. Appl. Phys.*, 2013, **13**, 841-845.

[51] J.-H. Shin and J. H. Moon, *Langmuir*, 2011, **27**, 6311-6315.

[52] J.-H. Shin, J.-H. Kang, W.-M. Jin, J. H. Park, Y.-S. Cho and J. H. Moon, *Langmuir*, 2011, **27**, 856-860.

[53] A. Mihi, M. E. Calvo, J. A. Anta and H. Míguez, *J. Phys. Chem. C*, 2008, **112**, 13-17.

[54] J. Xiao, Q. Huang, J. Xu, C. Li, G. Chen, Y. Luo, D. Li and Q. Meng, *J. Phys. Chem. C*, 2014, **118**, 4007-4015.

[55] C. L. Huisman, J. Schoonman and A. Goossens, *Sol. Energy Mater. Sol. Cells*, 2005, **85**, 115-124.

[56] E. S. Kwak, W. Lee, N.-G. Park, J. Kim and H. Lee, *Adv. Funct. Mater.*, 2009, **19**, 1093-1099.

[57] L. Qi, J. D. Sorge and D. P. Birnie Iii, *J. Am. Ceram. Soc.*, 2009, **92**, 1921-1925.

[58] G. Ruani, C. Ancora, F. Corticelli, C. Dionigi and C. Rossi, *Sol. Energy Mater. Sol. Cells*, 2008, **92**, 537-542.

[59] Y. G. Seo, K. Woo, J. Kim, H. Lee and W. Lee, *Adv. Funct. Mater.*, 2011, **21**, 3094-3103.

[60] S.-H. Han, S. Lee, H. Shin and H. S. Jung, *Adv. Energy Mater.*, 2011, **1**, 546-550.

[61] F. E. Osterloh, *Chem. Soc. Rev.*, 2013, **42**, 2294-2320.

[62] M. Guo, K. Xie, J. Lin, Z. Yong, C. T. Yip, L. Zhou, Y. Wang and H. Huang, *Energy Environ. Sci.*, 2012, **5**, 9881-9888.

[63] C. T. Yip, H. Huang, L. Zhou, K. Xie, Y. Wang, T. Feng, J. Li and W. Y. Tam, *Adv. Mater.*, 2011, **23**, 5624-5628.

[64] E. Macia, *Rep. Prog. Phys.*, 2012, **75**, 036502.

[65] A. Arie and N. Voloch, *Laser Photon. Rev.*, 2010, **4**, 355-373.

[66] A. Endo and Y. Iye, *Phys. Rev. B*, 2008, **78**, 085311.

[67] B. Mandlmeier, J. M. Szeifert, D. F.-Rohlfing, H. Amenitsch and T. Bein, *J. Am. Chem. Soc.*, 2011, **133**, 17274-17282.

[68] M. Guo, K. Y. Xie, Y. Wang, L. Zhou and H. Huang, *Sci. Rep.*, 2014, **4**, 6442.

[69] S. Matsushita, O. Suavet and H. Hashiba, *Electrochim. Acta*, 2010, 55, 2398.

[70] S. Matsushita, M. Hayashi, T. Isobe and A. Nakajima, *Crystals*, 2012, **2**, 1483-1491.

[71] A. Matsutani, M. Hayashi, Y. Morii, K. Nishioka, T. Isobe, A. Nakajima and S. Matsushita, *Jpn. J. Appl. Phys.*, 2012, 51, 098002

[72] M. E. Calvo, S. Colodrero, N. Hidalgo, G. Lozano, C. L.-López, O. S.-Sobrado and H. Míguez, *Energy Environ. Sci.*, 2011, **4**, 4800-4812.

[73] C. L.-López, S. Colodrero, M. E. Calvo and H. Míguez, *Energy Environ. Sci.*, 2013, **6**, 1260-1266.

[74] S. Colodrero, M.Ocana and H. Míguez, *Langmuir*, 2008, **24**, 4430-4434.

[75] M. E. Calvo, O. S.-Sobrado, S. Colodrero and H. Míguez, *Langmuir*, 2009, **25**, 2443-2448.

[76] G. Lozano, S. Colodrero, O. Caulier, M. E. Calvo and H. Míguez, *J. Phys. Chem. C*, 2010, **114**, 3681-3687.

[77] S. Guldin, M. Kolle, M. Stefik, R. Langford, D. Eder, U. Wiesner and U. Steiner, *Adv. Mater.*, 2011, **23**, 3664-3668.

[78] G. Subramania, K. Constant, R. Biswas, M. M. Sigalas and K. M. Ho, *Adv. Mater.*, 2001, **13**, 443-446.

[79] C. H. Yip, Y. M. Chiang and C.C . Wong, *J. Opt. Soc. Am. B*, 201, **27**, 920-926.

[80] M. Peters, J. C. Goldschmidt, P. Löper, B. Groß, J. Üpping, F. Dimroth, R. B. Wehrspohn and B. Bläsi, *Energies*, 2010, **3**, 171-193.

[81] J. Lin, K. Liu and X. Chen, *Small*, 2011, **7**, 1784-1789.

[82] M. Guo, Z. Yong, K. Xie, J. Lin, Y. Wang and H. Huang, *ACS Appl. Mater. Interfaces*, 2013, **5**, 13022-13028.

[83] A. Mihi and H. Míguez, *J. Phys. Chem. B*, 2005, **109**, 15968-15976.

[84] A. Mihi, F. J. L.-Alcaraz and H. Míguez, *Appl. Phys. Lett.*, 2006, **88**, 193110.

[85] V. K. Narasimhan and Y. Cui, *Nanophotonics*, 2013, **2**, 187-210.

[86] B. Lee, D. K. Hwang, P. Guo, S. T. Ho, D. B. Buchholtz, C. Y. Wang and R. P. Chang, *J. Phys. Chem. B*, 2010, **114**, 14582-14591.

[87] M. Guo, K. Xie, X. Liu, Y. Wang, L. Zhou and H. Huang, *Nanoscale*, 2014, **6**, 13060-13067.

[88] K. Y. Xie, M. Guo, X. L. Liu and H. T. Huang, *J. Power Sources*, 2015, **293**, 170-177.

[89] D. Colonna, S. Colodrero, H. Lindstrom, A. Di Carlo and H. Miguez, *Energy Environ. Sci.*, 2012, **5**, 8238-8243.

[90] A. Mihi, S. Colodrero, M. Calvo, M. Ocana and H. Miguez, Active Photonic Crystals, *Proceedings of SPIE*, 2007, **6640**, art.no.664007, Edited by S. M. Weiss, G. S. Subramania and F. G.-Santamaria.

[91] L. Liu, S. K. Karuturi, L. T. Su and A. I. Y. Tok, *Energy Environ. Sci.*, 2011, **4**, 209-215.

[92] M. Jin, S. S. Kim, M. Yoon, Z. Li, Y. Y. Lee and J. M. Kim, *J. Nanosci. Nanotech.*, 2012, **12**, 815-821.

[93] H. Li, X. Hu, W. Hong, F. Cai, Q. Tang, B. Zhao, D. Zhang and P. Cheng, *Phys. Chem. Chem. Phys.*, 2012, **14**, 14334-14339.

[94] J.-H. Choi, S.-H. Kwon, Y.-K. Jeong, I. Kim and K.-H. Kim, *J. Electrochem. Soc.*, 2011, **158**, B749-753.

[95] C.-Y. Cho and J. H. Moon, *Langmuir*, 2012, **28**, 9372-9377.

[96] H.-N. Kim and J. H. Moon, *ACS Appl. Mater. Interfaces*, 2012, **4**, 5821-5825.

[97] J. Y. Lee, S. Lee, J. K. Park, Y. Jun, Y. G. Lee, K. M. Kim, J. H. Yun and K. Y. Cho, *Opt Express*, 2010, **18** Suppl 4, A522-527.

[98] Y. H. Jang and D. H. Kim, *Nanoscale*, 2014, **6**, 4204-4210.

[99] D.-Y. Kang, Y. Lee, C.-Y. Cho and J. H. Moon, *Langmuir*, 2012, **28**, 7033-7038.

[100] J. T. Park, W. S. Chi, S. J. Kim, D. Lee and J. H. Kim, *Sci. Reports*, 2014, **4**, 5505.

[101] S. Zhang, G.-Y. Dong, B. Lin, J. Qu, N.-Y. Yuan and J.-N. Ding, *J. Power Sources*, 2015, **277**, 52-58.

[102] G. Kato, C. Nishiyama, T. Yabuta, M. Miyauchi, T. Hashimoto, T. Isobe, A. Nakajima and S. Matsushita, *J. Porous Mater.*, 2014, **21**, 165-176.

[103] D. W. Park, Y. Jeong, T. PremKumar and J. Lee, *ACS App. Mater. Inter.*, 2014, **6**, 14399-14404.

[104] H. K. Jun, M. A. Careem and A. K. Arof, *Renew. Sustain. Energy Rev.*, 2013, **22**, 148-167.

[105] T. Toyoda and Q. Shen, *J. Phys. Chem. Lett.*, 2012, **3**, 1885-1893.

[106] S. Bayram and L. Halaoui, *Particle Particle Sys. Charact.*, 2013, **30**, 706-714.

[107] H. J. Snaith, *J. Phys. Chem. Lett.*, 2013, **4**, 3623-3630.

[108] B. E. Hardin, H. J. Snaith and M. D. McGehee, *Nat. Photon.*, 2012, **6**, 162-169.

[109] H. Zhou, Q. Chen, G. Li, S. Luo, T. B. Song, H. S. Duan, Z. Hong, J. You, Y. Liu and Y. Yang, *Science*, 2014, **345**, 542-546.

[110] J. H. Heo, S. H. Im, J. H. Noh, T. N. Mandal, C. S. Lim, J. A. Chang, Y. H. Lee, H. J. Kim, A. Sarkar, M. K. Nazeeruddin, M. Gratzel and S. I. Seok, *Nat. Photon.*, 2013, **7**, 487-492.

[111] M. M. Lee, J. Teuscher, T. Miyasaka, T. N. Murakami and H. J. Snaith, *Science*, 2012, **338**, 643-647.

[112] N. J. Jeon, J. H. Noh, W. S. Yang, Y. C. Kim, S. Ryu, J. Seo and S. I. Seok, *Nature*, 2015, 517, 476-480.

[113] M. A. Green, A. H.-Baillie and H. J. Snaith, *Nat. Photon.*, 2014, **8**, 506-514.

[114] W. Y. Nie, H. H. Tsai, R. Asadpour, J. C. Blancon, A. J. Neukirch, G. Gupta, J. J. Crochet, M. Chhowalla, S. Tretiak, M. A. Alam, H. L. Wang and A. D. Mohite, *Science*, 2015, **347**, 522-525.

[115] Q. Q. Lin, A. Armin, R. C. R. Nagiri, P. L. Burn and P. Meredith, *Nat. Photon.*, 2015, **9**, 106-112.

[116] D. Y. Liu and T. L. Kelly, *Nat. Photon.*, 2014, **8**, 133-138.

[117] W. Zhang, M. Anaya, G. Lozano, M. E. Calvo, M. B. Johnston, H. Miguez and H. J. Snaith, *Nano Lett.*, 2015, **15**, 1698-1702.

[118] S. Linic, P. Christopher and D. B. Ingram, *Nat. Mater.*, 2011, **10**, 911-921.

[119] V. E. Ferry, J. N. Munday and H. A. Atwater, *Adv. Mater.*, 2010, **22**, 4794-4808.

[120] G. Zhao, H. Kozuka and T. Yoko, *Sol. Energy Mater. Sol. Cells*, 1997, **46**, 219-231.

[121] C.Wen, K. Ishikawa, M. Kishima and K. Yamada, *Sol. Energy Mater. Sol. Cells*, 2000, **61**, 339-351.

[122] S. D. Standridge, G. C. Schatz and J. T.Hupp, *Langmuir* 2009, **25**, 2596-2600.

[123] W. H. Lai, Y. H. Su, L. G. Teoh and M. H. Hon, *J. Photochem. Photobiol. A*, 2008, **195**, 307-313.

[124] J. F. Qi, X. N. Dang, P. T. Hammond and A. M. Belcher, *ACS Nano*, 2011, **5**, 7108-7116.

[125] H. Choi, W. T. Chen and P. V. Kamat, *ACS Nano*, 2012, **6**, 4418-4427.

[126] J. G. Smith, J. A. Faucheaux and P. K. Jain, *Nano Today*, 2015, **10**, 67-80.

**Table of contents entry**

The fabrication strategies, optical properties of photonic crystals are reviewed with a focus on their application in sensitized solar cells.